Meta-analysis of virus-induced host gene expression reveals unique signatures of immune dysregulation induced by SARS-CoV-2

Srikeerthana Kuchi, Quan Gu, Massimo Palmarini, Sam J Wilson, David L Robertson

MRC-University of Glasgow Centre for Virus Research (CVR), Glasgow, UK.

Corresponding authors: Srikeerthana.Kuchi@glasgow.ac.uk, david.l.robertson@glasgow.ac.uk

Abstract

The clinical outcome of COVID-19 has an extreme age, genetic and comorbidity bias that is thought to be driven by an impaired immune response to SARS-CoV-2, the causative agent of the disease. The unprecedented impact of COVID-19 on global health has resulted in multiple studies generating a variety of large gene expression datasets in a relatively short period of time. In order to better understand the immune dysregulation induced by SARS-CoV-2, we carried out a meta-analysis of these transcriptomics data available in the published literature. Datasets included both those available from SARS-CoV-2 infected cell lines *in vitro* and those from patient samples. We focused our analysis on the identification of viral perturbed host functions as captured by co-expressed gene module analysis. Transcriptomics data from lung biopsies and nasopharyngeal samples, as opposed to those available from other clinical samples and infected cell lines, provided key signatures on the role of the host's immune response on COVID-19 pathogenesis. For example, severity of infection and patients' age are linked to the absence of stimulation of the RIG-I-like receptor signaling pathway, a known critical immediate line of defense against RNA viral infections that triggers type-I interferon responses. In addition, co-expression analysis of age-stratified transcriptional data provided evidence that signatures of key immune response pathways are perturbed in older COVID-19 patients. In particular, dysregulation of antigen-presenting components, down-regulation of cell cycle mechanisms and signatures of hyper-enriched monocytes were strongly correlated with the age of older individuals infected with SARS-CoV-2. Collectively, our meta-analysis highlights the ability of transcriptomics and gene-module analysis of aggregated datasets to aid our improved understanding of the host-specific disease mechanisms underpinning COVID-19.

Introduction

Coronavirus disease 2019 (COVID-19) is caused by SARS-CoV-2 (severe acute respiratory syndrome coronavirus 2), a new coronavirus phylogenetically related to two other coronaviruses that emerged in the last 20 years: SARS-CoV (referred to as SARS-CoV-1 here for clarity) and MERS-CoV (Middle East respiratory syndrome coronavirus). SARS-CoV-2, like SARS-CoV-1, utilises ACE2 (angiotensin converting enzyme II) for cellular entry using its spike (S) protein (Zhou et al. 2020). The SARS-CoV-2 S-protein contains a polybasic cleavage site and is estimated to bind ACE2 with 10-20 fold higher affinity than SARS-CoV-1 spike, contributing to infection success, particularly in the upper respiratory tract, by making cells with lower ACE2 expression levels more accessible (Wrapp et al. 2020). Globally, as of December 2020, SARS-CoV-2 has caused over 1.7M recorded deaths. The majority of SARS-CoV-2 infected individuals are asymptomatic or display relatively mild symptoms including fever, cough and temporary anosmia (loss of the sense of smell). More severe cases can include symptoms associated with acute respiratory distress syndrome (ARDS), circulatory and heart problems, organ failure and death (Huang et al. 2020).

The severity of COVID-19 is highly correlated with age and certain comorbidities (Pinto et al. 2020) and has been associated with immune defects (Pairo-Castineira et al. 2020). Virulent SARS-CoV-2 infections are associated with a dysfunctional immune response and "cytokine storm" is a particular marker of disease severity. For example, transcriptomics of BALF (bronchoalveolar lavage fluid) and PBMC (peripheral blood mononuclear cells) demonstrated extensive upregulation of cytokines in COVID-19 patients (Xiong et al. 2020). Moreover, it has been shown that SARS-CoV-2 infection *in vitro* triggers cGAS-STING mediated NF-κB response and a pro-inflammatory cytokine response (Neufeldt et al. 2020). Type I interferons (IFN) likely play a pivotal role in SARS-CoV-2 pathogenesis as genetic mutations in the IFN system and autoantibodies to type I IFNs predispose individuals to severe COVID-19 disease (Bastard et al. 2020, Zhang et al. 2020). Understanding the immune and inflammatory responses to SARS-CoV-2 is, thus, crucial to deciphering the mechanisms of viral pathogenesis.

Here we carry out a detailed meta-analysis of available SARS-CoV-2 transcriptomics (RNA-Seq) datasets and focus on the relationships among groups of differentially expressed genes in order to enable comparison between distinct studies. Transcriptomics of virus-infected cells can help us to understand how genes are regulated under specific biological conditions in the context of viral infection. 'Gene sets' are groups of genes that are co-expressed as they contribute to a shared biological function, for example, a signaling pathway up-regulated by virus infection. Gene sets associated with specific conditions, in this case viral infection, are usually derived from multiple studies and their activity under different conditions provides a way to extract biological relationships from large disparate transcriptomics datasets. Gene set tests enable us to analyze groups of genes that represent biological functions as a group rather than individual differentially expressed genes. Gene sets therefore are particularly helpful in meta-analysis of transcriptomics data from different sources. Competitive gene set testing methods such as gene set enrichment analysis (GSEA) (Subramanian et al. 2005) evaluate the statistical significance of enrichment by determining whether a set of genes are correlated to the diseased state compared to genes in other gene sets, while self-contained methods such as ROAST (Wu et al. 2010) evaluate whether any genes within a gene set are differentially expressed, allowing testing for co-regulated genes.

In order to investigate transcriptional responses to SARS-CoV-2 infection in COVID-19 patients and to compare transcriptional signatures elicited by SARS-CoV-1 and MERS-CoV, we use a well-refined gene set established as 'blood transcriptome modules' (BTMs), defined by Li and co-workers using large scale network integration of public data and context specific biological information (Li et al. 2014). While biological pathway based analysis focuses primarily on chains of interacting molecules perturbed in complex diseases such as cancer, BTMs provide high resolution gene modules that better represent the groups of molecules activated by host immunological responses (Li et al. 2016). Modules in BTMs are derived by gene co-expression patterns, supported by experimental information derived from various tissues, cell-types, interactome studies and molecular pathway information. As with canonical pathways, BTMs can be applied to transcriptomics datasets derived from various tissues and cell lines in order to better understand host responses triggered by infection. Higher classification of these functional modules into groups (Kazmin et al. 2017) based on the pathways or the cell lineages can be used to systematically capture altering responses to examine the differences in modules that have a common biological function or regulation. We also use the biological pathway software

Ingenuity Pathway Analysis (IPA) to compare signaling pathways among the various data sets. To identify the co-expressed networks of genes associated with viral load and different age groups in a large dataset of SARS-CoV-2 infected individuals (Lieberman et al. 2020), we apply the weighted gene correlation network analysis (WGCNA), a well-developed co-expression method. By correlating groups of genes with BTMs, we assess the functional role of these networks in infected individuals and provide systems-level evidence of the networks that contribute to the pathology of the disease in different age groups.

Results

SARS-CoV-2 elicits signatures of adaptive immune pathways in cell lines. In order to assess the genes associated with the transcriptional dysregulation induced by SARS-CoV-2 in infected cell lines, we compared differential module enrichment profiles to the available SARS-CoV-1 and MERS-CoV time-matched cell line data. We find SARS-CoV-2 has a distinct module enrichment profile compared to SARS-CoV-1 and MERS-CoV in the different cell lines analysed, confirming previous analysis (Blanco-Melo et al. 2020). In Calu-3 cells, SARS-CoV-2 exhibits a profound upregulation of all essential B-cell modules (M47.4, M47.3, M54, M9, M58) at 24 hours post infection relative to SARS-CoV-1, while MERS-CoV elicits a complementary B-cell response in Calu-3 cell lines (figure 1), similar to B-cell module enrichment by SARS-CoV-1 and MERS-CoV in MRC5 cell lines.

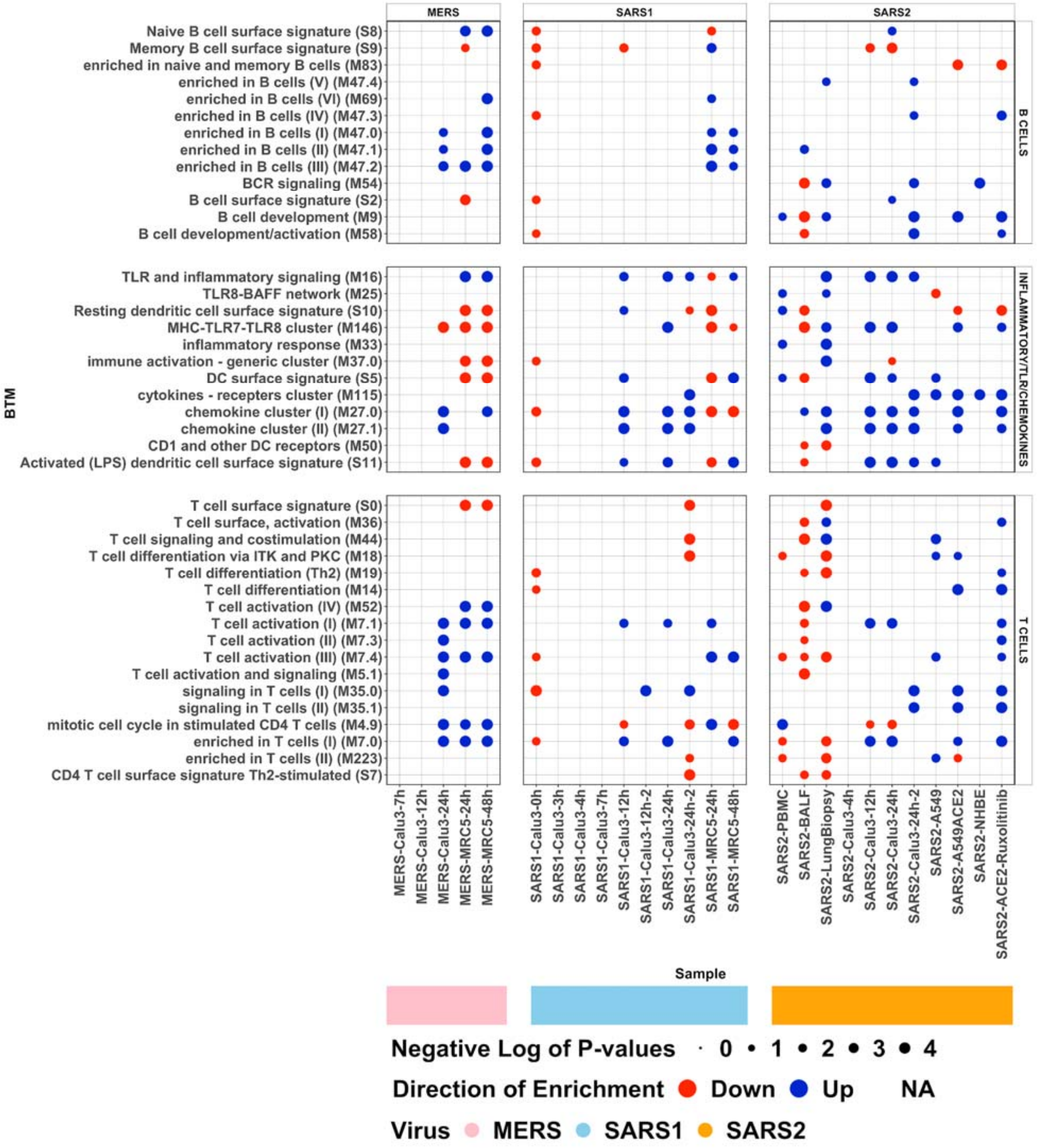

Figure 1. Plot showing -log10(p-values) of differentially enriched B cell, Inflammatory/TLR/Chemokine and T cell modules (y-axis) for different transcriptome datasets (x-axis), see Table 1. The size of the circles corresponds to the magnitude of the -log10(p-value), while their colour corresponds to the direction of enrichment as indicated by the MROAST R package (see key).

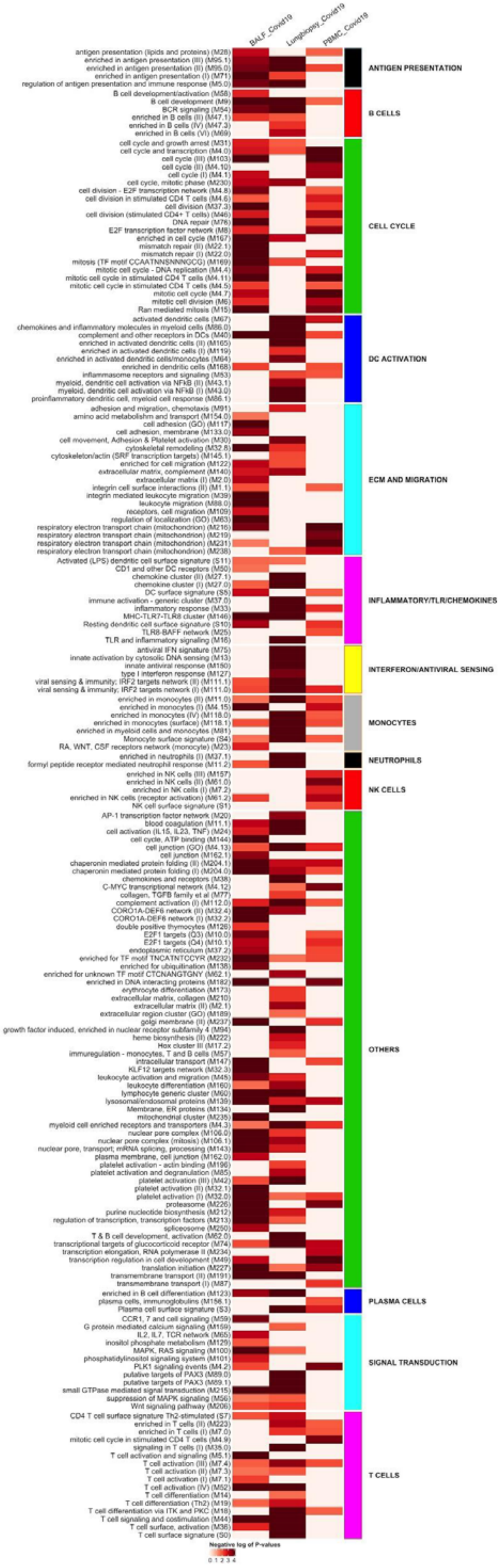
BALF_Covid19
Lungbiopsy_Covid19
PBMC_Covid19
antigen presentation (lipids and proteins) (M28)
enriched in antigen presentation (III) (M95.1)
enriched in antigen presentation (II) (M95.0)
enriched in antigen presentation (I) (M71)
regulation of antigen presentation and immune response (M5.0)
ANTIGEN PRESENTATION
B cell development/activation (M58)
B cell development (M9)
BCR signaling (M54)
enriched in B cells (II) (M47.1)
enriched in B cells (IV) (M47.3)
enriched in B cells (VI) (M69)
B CELLS
cell cycle and growth arrest (M31)
cell cycle and transcription (M4.0)
cell cycle (III) (M103)
cell cycle (II) (M4.10)
cell cycle (I) (M4.1)
cell cycle, mitotic phase (M230)
cell division - E2F transcription network (M4.8)
cell division in stimulated CD4 T cells (M4.6)
cell division (M37.3)
cell division (stimulated CD4+ T cells) (M46)
DNA repair (M76)
E2F transcription factor network (M8)
enriched in cell cycle (M167)
mismatch repair (II) (M22.1)
mismatch repair (I) (M22.0)
mitosis (TF motif CCAATNNSNNNGCG) (M169)
mitotic cell cycle - DNA replication (M4.4)
mitotic cell cycle in stimulated CD4 T cells (M4.11)
mitotic cell cycle in stimulated CD4 T cells (M4.5)
mitotic cell cycle (M4.7)
mitotic cell division (M6)
Ran mediated mitosis (M15)
CELL CYCLE
activated dendritic cells (M67)
chemokines and inflammatory molecules in myeloid cells (M86.0)
complement and other receptors in DCs (M40)
enriched in activated dendritic cells (II) (M165)
enriched in activated dendritic cells (I) (M119)
enriched in activated dendritic cells/monocytes (M64)
enriched in dendritic cells (M168)
inflammasome receptors and signaling (M53)
myeloid, dendritic cell activation via NFkB (II) (M43.1)
myeloid, dendritic cell activation via NFkB (I) (M43.0)
proinflammatory dendritic cell, myeloid cell response (M86.1)
DC ACTIVATION
adhesion and migration, chemotaxis (M91)
amino acid metabolishm and transport (M154.0)
cell adhesion (GO) (M117)
cell adhesion, membrane (M133.0)
cell movement, Adhesion & Platelet activation (M30)
cytoskeletal remodeling (M32.8)
cytoskeleton/actin (SRF transcription targets) (M145.1)
enriched for cell migration (M122)
extracellular matrix, complement (M140)
extracellular matrix (I) (M2.0)
integrin cell surface interactions (II) (M1.1)
integrin mediated leukocyte migration (M39)
leukocyte migration (M88.0)
receptors, cell migration (M109)
regulation of localization (GO) (M63)
respiratory electron transport chain (mitochondrion) (M216)
respiratory electron transport chain (mitochondrion) (M219)
respiratory electron transport chain (mitochondrion) (M231)
respiratory electron transport chain (mitochondrion) (M238)
ECM AND MIGRATION
Activated (LPS) dendritic cell surface signature (S11)
CD1 and other DC receptors (M50)
chemokine cluster (II) (M27.1)
chemokine cluster (I) (M27.0)
DC surface signature (S5)
immune activation - generic cluster (M37.0)
inflammatory response (M33)
MHC-TLR7-TLR8 cluster (M146)
Resting dendritic cell surface signature (S10)
TLR8-BAFF network (M25)
TLR and inflammatory signaling (M16)
INFLAMMATORY/TLR/CHEMOKINES
antiviral IFN signature (M75)
innate activation by cytosolic DNA sensing (M13)
innate antiviral response (M150)
type I interferon response (M127)
viral sensing & immunity; IRF2 targets network (II) (M111.1)
viral sensing & immunity; IRF2 targets network (I) (M111.0)
INTERFERON/ANTIVIRAL SENSING
enriched in monocytes (II) (M11.0)
enriched in monocytes (I) (M4.15)
enriched in monocytes (IV) (M118.0)
enriched in monocytes (surface) (M118.1)
enriched in myeloid cells and monocytes (M81)
Monocyte surface signature (S4)
RA, WNT, CSF receptors network (monocyte) (M23)
MONOCYTES
enriched in neutrophils (I) (M37.1)
formyl peptide receptor mediated neutrophil response (M11.2)
NEUTROPHILS
enriched in NK cells (III) (M157)
enriched in NK cells (II) (M61.0)
enriched in NK cells (I) (M7.2)
enriched in NK cells (receptor activation) (M61.2)
NK cell surface signature (S1)
NK CELLS
AP-1 transcription factor network (M20)
blood coagulation (M11.1)
cell activation (IL15, IL23, TNF) (M24)
cell cycle, ATP binding (M144)
cell junction (GO) (M4.13)
cell junction (M162.1)
chaperonin mediated protein folding (II) (M204.1)
chaperonin mediated protein folding (I) (M204.0)
chemokines and receptors (M38)
C-MYC transcriptional network (M4.12)
collagen, TGFB family et al (M77)
complement activation (I) (M112.0)
CORO1A-DEF6 network (II) (M32.4)
CORO1A-DEF6 network (I) (M32.2)
double positive thymocytes (M126)
E2F1 targets (Q3) (M10.0)
E2F1 targets (Q4) (M10.1)
endoplasmic reticulum (M37.2)
enriched for TF motif TNCATNTCCYR (M232)
enriched for ubiquitination (M138)
enriched for unknown TF motif CTCNANGTGNY (M62.1)
enriched in DNA interacting proteins (M182)
erythrocyte differentiation (M173)
extracellular matrix, collagen (M210)
extracellular matrix (II) (M2.1)
extracellular region cluster (GO) (M189)
golgi membrane (II) (M237)
growth factor induced, enriched in nuclear receptor subfamily 4 (M94)
heme biosynthesis (II) (M222)
Hox cluster III (M17.2)
immuregulation - monocytes, T and B cells (M57)
intracellular transport (M147)
KLF12 targets network (M32.3)
leukocyte activation and migration (M45)
leukocyte differentiation (M160)
lymphocyte generic cluster (M60)
lysosomal/endosomal proteins (M139)
Membrane, ER proteins (M134)
mitochondrial cluster (M235)
myeloid cell enriched receptors and transporters (M4.3)
nuclear pore complex (M106.0)
nuclear pore complex (mitosis) (M106.1)
nuclear pore, transport; mRNA splicing, processing (M143)
plasma membrane, cell junction (M162.0)
platelet activation - actin binding (M196)
platelet activation and degranulation (M85)
platelet activation (III) (M42)
platelet activation (II) (M32.1)
platelet activation (I) (M32.0)
proteasome (M226)
purine nucleotide biosynthesis (M212)
regulation of transcription, transcription factors (M213)
spliceosome (M250)
T & B cell development, activation (M62.0)
transcriptional targets of glucocorticoid receptor (M74)
transcription elongation, RNA polymerase II (M234)
transcription regulation in cell development (M49)
translation initiation (M227)
transmembrane transport (II) (M191)
transmembrane transport (I) (M87)
OTHERS
enriched in B cell differentiation (M123)
plasma cells, immunoglobulins (M156.1)
Plasma cell surface signature (S3)
PLASMA CELLS
CCR1, 7 and cell signaling (M59)
G protein mediated calcium signaling (M159)
IL2, IL7, TCR network (M65)
inositol phosphate metabolism (M129)
MAPK, RAS signaling (M100)
phosphatidylinositol signaling system (M101)
PLK1 signaling events (M4.2)
putative targets of PAX3 (M89.0)
putative targets of PAX3 (M89.1)
small GTPase mediated signal transduction (M215)
suppression of MAPK signaling (M56)
Wnt signaling pathway (M206)
SIGNAL TRANSDUCTION
CD4 T cell surface signature Th2-stimulated (S7)
enriched in T cells (II) (M223)
enriched in T cells (I) (M7.0)
mitotic cell cycle in stimulated CD4 T cells (M4.9)
signaling in T cells (I) (M35.0)
T cell activation and signaling (M5.1)
T cell activation (III) (M7.4)
T cell activation (II) (M7.3)
T cell activation (I) (M7.1)
T cell activation (IV) (M52)
T cell differentiation (M14)
T cell differentiation (Th2) (M19)
T cell differentiation via ITK and PKC (M18)
T cell signaling and costimulation (M44)
T cell surface, activation (M36)
T cell surface signature (S0)
T CELLS
Negative log of P-values
0 1 2 3 4

Figure 2. Heatmap of -log10(p-values) of the differentially enriched modules of PBMC, BALF and lung biopsy samples. High level annotation of each module (row) is represented by the classification assigned by Kazmin et al. (2017) based on pathways or cell lineage each module represents. Direction of enrichment of the modules are shown in supplementary figure 1.

Interestingly, while MERS-CoV exhibits a ‘strong’ upregulation of T-cell modules in Calu-3 and MRC5 cell lines at 24 hours post infection, both the SARS-CoV-1 and -2 demonstrate a weak T-cell response signature in both cell lines, indicating a failure of the SARS viruses to trigger genes associated with adaptive immune/innate T cell responses. ACE2 transduced A549 cells and ACE2 transduced Ruxolitinib treated A549 cells show a strong enrichment of T-cell modules, while A549 and NHBE cells lacked significant enrichment of these modules. Both SARS-CoV-1 and 2 elicit a significant upregulation of the TLR (Toll-like receptors) and inflammatory signaling module (M16) in Calu-3 cells -- important in identifying different pathogen-associated molecular patterns (PAMPs) for the regulation of host innate immune response -- while MERS-CoV lacks a representation of this module consistent with MERS-CoV silencing the TLR response upon infection (Liang et al. 2020). All three betacoronavirus types exhibit evidence of a strong chemokine response (M27.1 and M27.0) in Calu-3 cells suggesting the activation of various cytokines to guide immune cell migration to the infection sites to elicit an active inflammatory response. SARS-CoV-2 is thus inducing a distinct transcriptional profile to both SARS-CoV-1 and MERS-CoV in infected cell lines.

Regulation of distinct functional modules exhibited by different clinical samples. A heatmap of the enrichment scores (negative log of p-values) of all dysregulated modules (figure 2) indicates that different clinical samples (Table 1 and supplementary table 1) from COVID-19 patients display distinct transcriptional responses upon SARS-CoV-2 infection. BTMs were categorized into groups by Kazmin et al. (2017) based on the common pathways or the cell lineages the genes represent. Analysis of these individual groups of the enriched modules show that, analogous to the severity of the disease, gene transcripts corresponding to the up-regulation of antigen presenting modules and dendritic cell activation modules, which are known to trigger strong innate immune response against respiratory infections, are upregulated in lung biopsy samples, while there is a profound down-regulation, or no significant regulation of these modules, in BALF samples (figure 3). Strikingly, there is an inverse correlation in the regulation status between PBMC and BALF samples in cell cycle related modules and no representation of these modules in lung biopsy samples. This is consistent with coronaviruses perturbing cell cycle mechanisms to evade detection by the host immune system in order to facilitate viral replication (Dove et al. 2006).

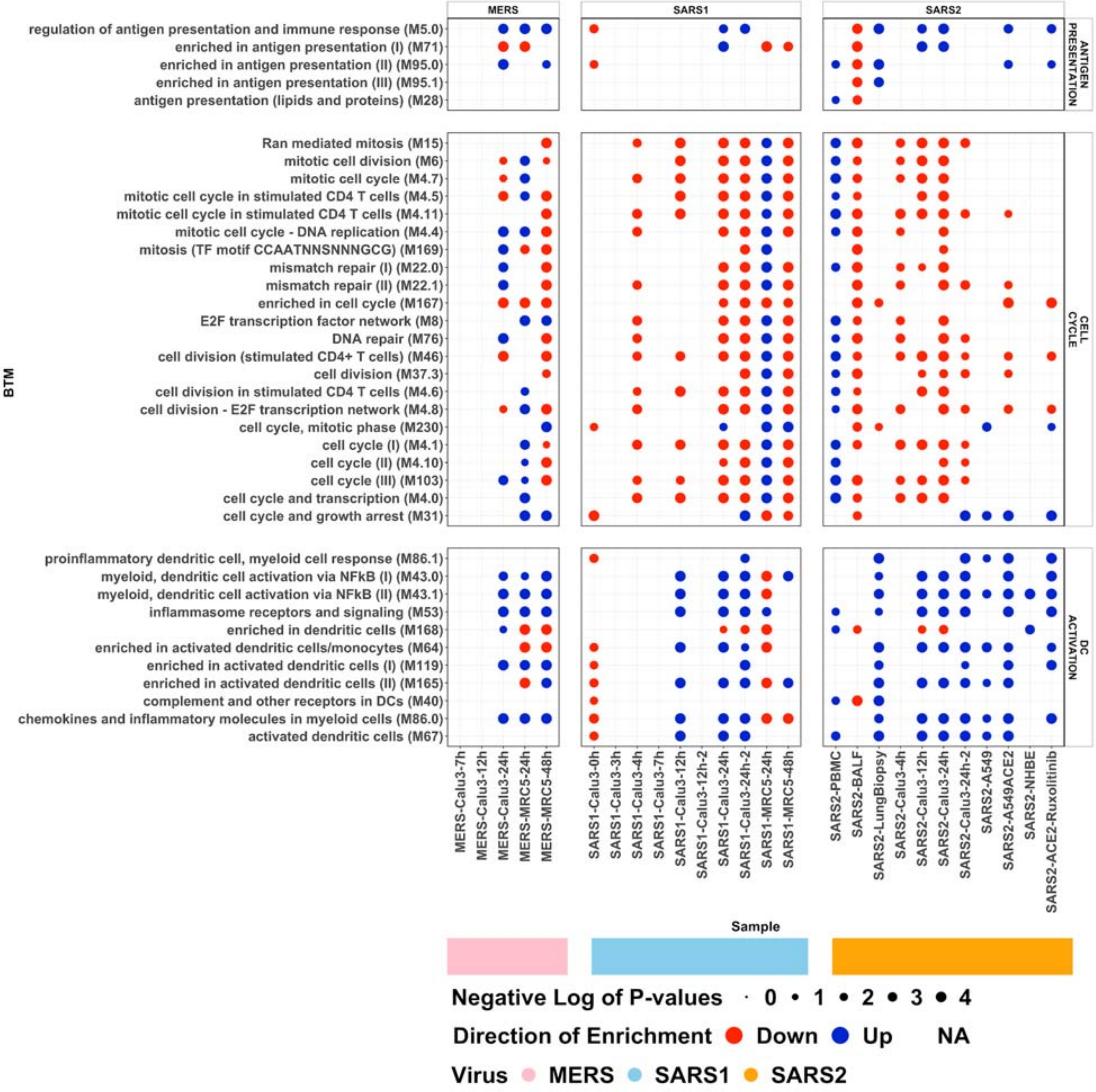

Figure 3. Plot showing -log10(p-values) of differentially enriched antigen presentation, cell cycle and DC activation modules (y-axis) for different transcriptome datasets (x-axis), see Table 1. The size of the circles corresponds to the magnitude of the -log10(p-value), while their colour corresponds to the direction of enrichment as indicated by the MROAST R package (see key).

To assess for transcriptional differences associated with age, we grouped 430 SARS-CoV-2 positive and 54 negative, samples, i.e., infected or uninfected, from the surveillance study (referred to here as surveillance data) of Lieberman et al. (2020) into groupings reflecting the viral load and age as follows: low (≤30, 31-60 and >60), med (≤30, 31-60 and >60), high (≤30, 31-60 and >60). Nasopharyngeal samples of the older infected individuals compared to the age-matched negative controls (samples from the uninfected individuals) exhibited a strong downregulation of cell cycle related modules in samples with either medium or low viral load (possibly relating to the later stages of infection) showing host physiology modification by the virus. Antigen-presenting dendritic cell (DC) related modules are upregulated in younger adults with high viral load (figure 4), correlating with the upregulation of dendritic cell activated T-cell modules (figure 5). Absence of the dysregulation of DC modules in older and younger individuals with low and medium viral load (figure 4) correlates with downregulation of some of the T-cell modules in these individuals (figure 5). It is important to note that irrespective of age, there is a profound downregulation of B-cell modules in all the samples with low viral load, while a crucial B cell development/activation module (M58) is downregulated only in older patients. Studies have previously shown that a subset of COVID-19 patients fail to develop long-lasting antibodies (Tay et al. 2020, Wang et al. 2020).

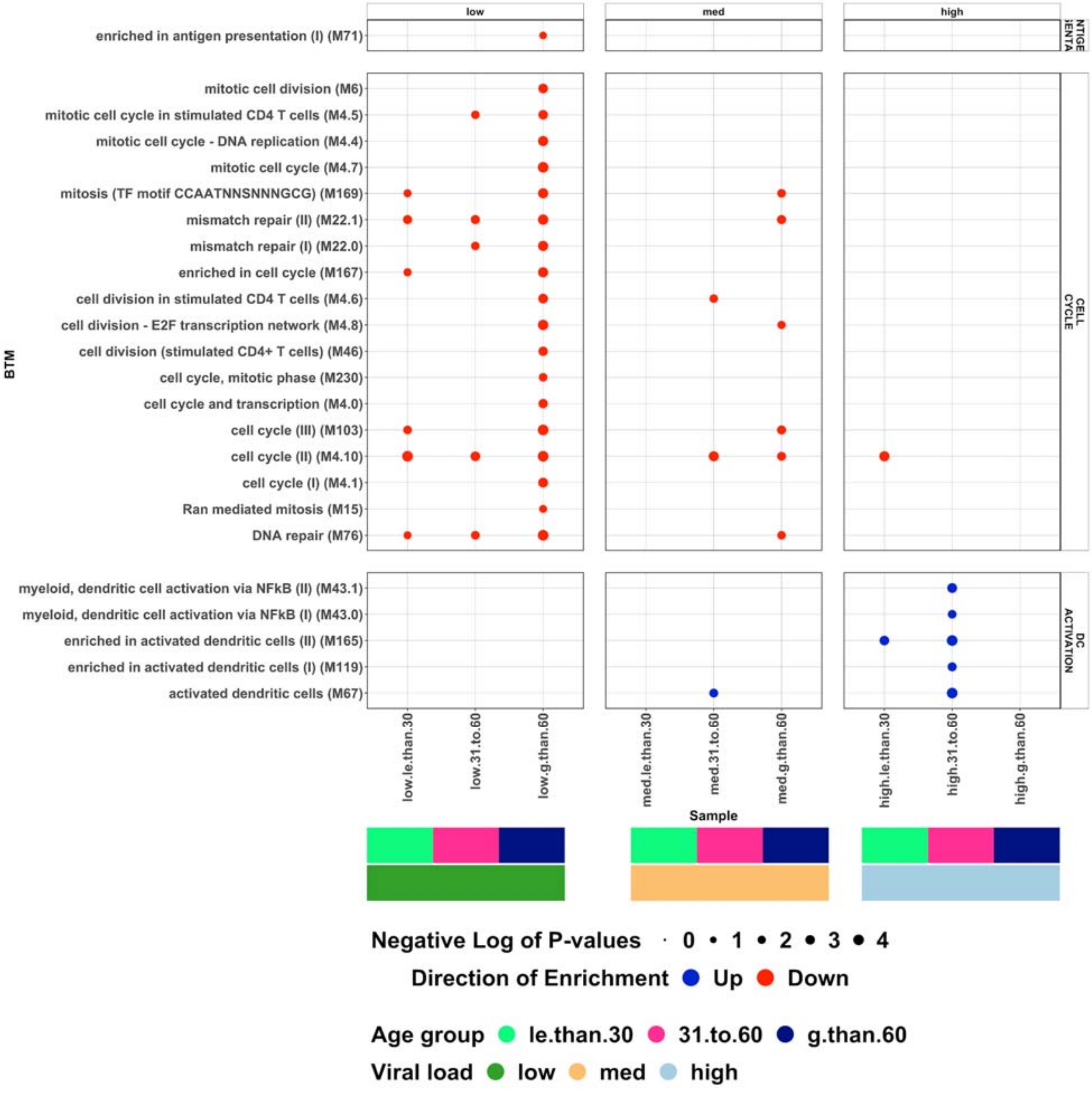

Figure 4. Plot showing -log10(p-values) of differentially enriched antigen presentation, cell cycle and DC activation modules (y-axis) of the surveillance data (Lieberman et al. 2020) stratified by age and viral load. The size of the circles corresponds to the magnitude of the -log10(p-value), while their colour corresponds to the direction of enrichment as indicated by mroast R package (see key).

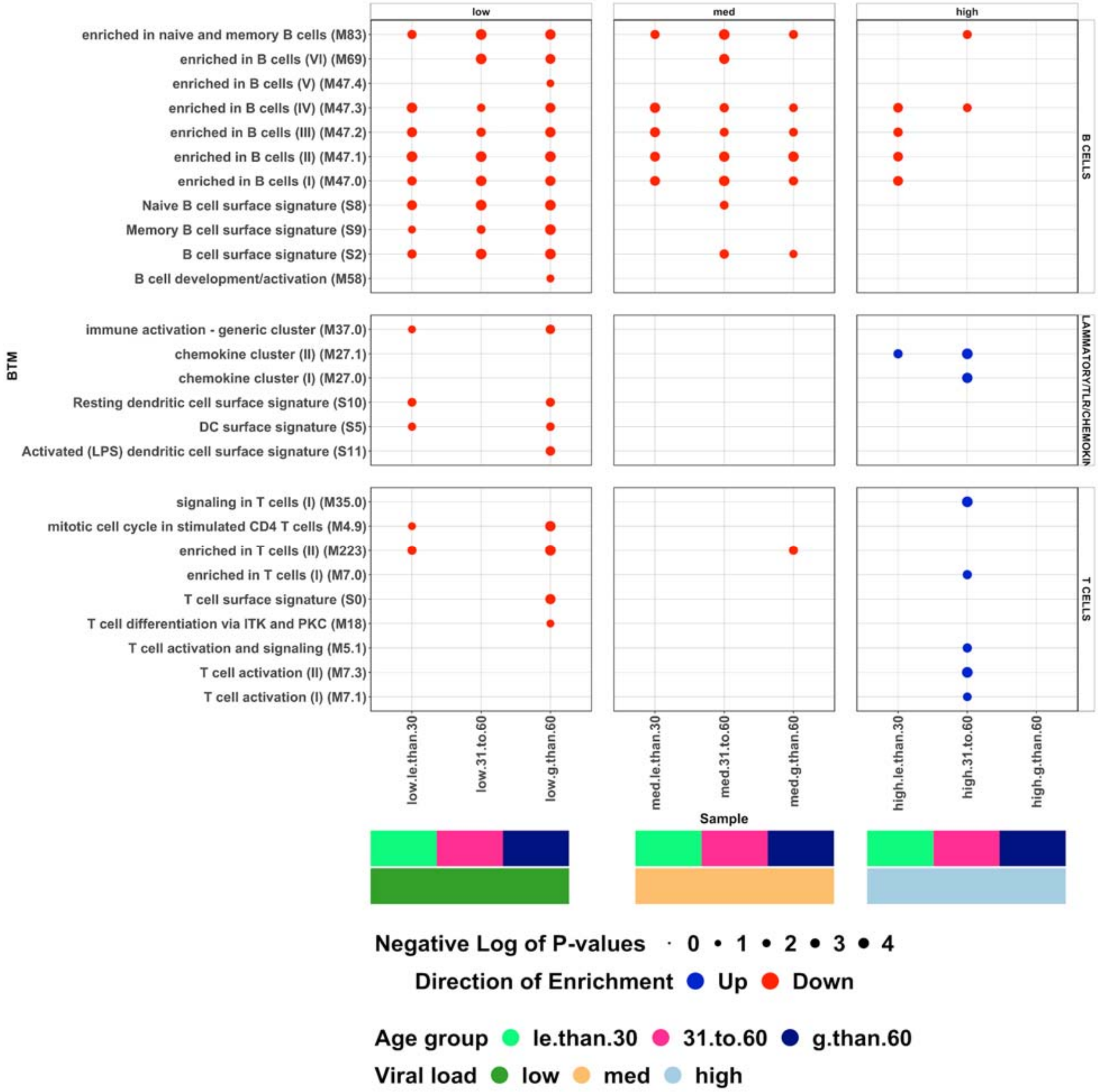

Figure 5. Plot showing -log10(p-values) of differentially enriched B cell, inflammatory/TLR/Chemokine and T cell modules (y-axis) of the surveillance data (Lieberman et al. 2020) stratified by age and viral load. The size of the circles corresponds to the magnitude of the -log10(p-value), while their colour corresponds to the direction of enrichment as indicated by mroast R package (see key).

With respect to inflammatory, TLR and chemokine modules, lung samples have a representation of chemokine clusters (M27.0 and M27.1), demonstrating an inflammatory response by the host system that's consistent with other studies (Huang et al. 2020, Zhao 2020, Mehta et al. 2020) while these modules are weakly enriched in BALF and completely absent in PBMC samples (figure 1). Heatmaps of log transformed scaled expression of the differentially regulated member genes of inflammatory, TLR and chemokine modules for Lung biopsy (and cell line) samples and PBMC-BALF samples are shown in supplementary figure 2 and 3, respectively. These data suggest that there is a strong upregulation of inflammatory genes in severely diseased COVID-19 patients.

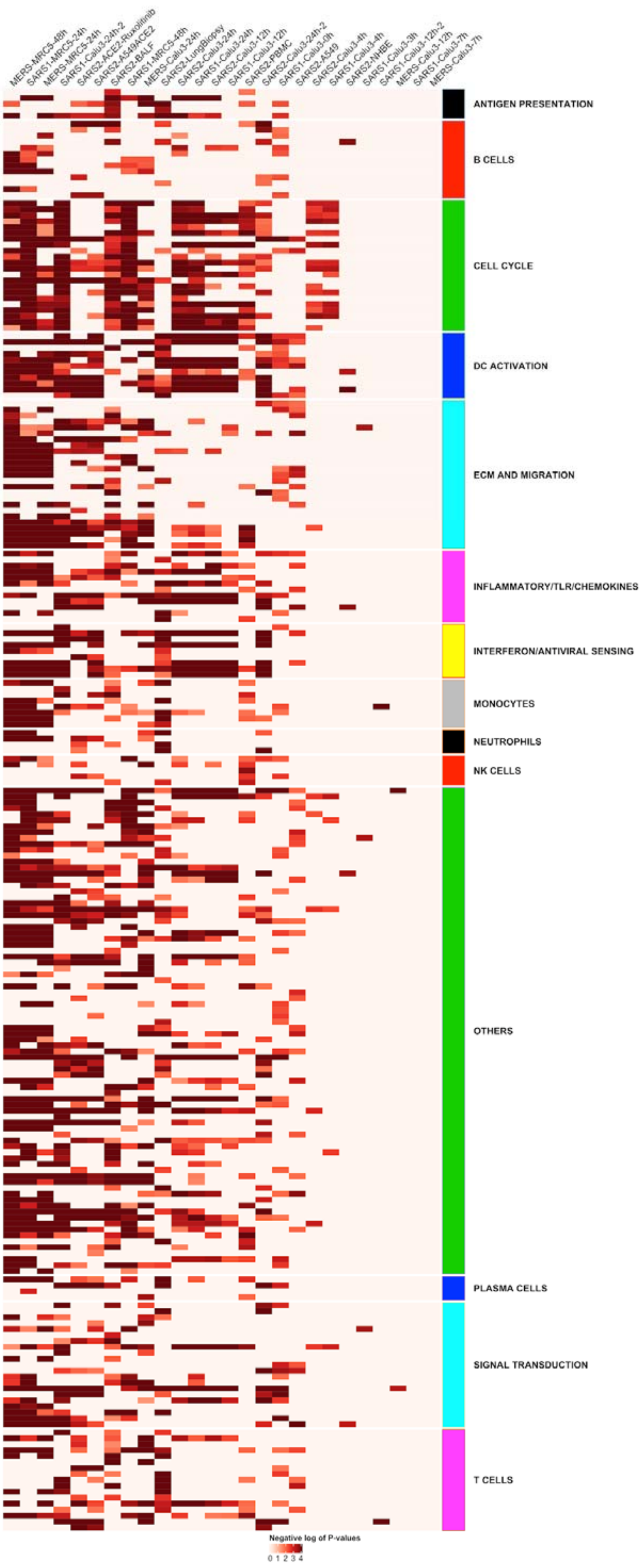
MERS-MRC5-48h
SARS1-MRC5-24h
MERS-MRC5-24h
SARS1-Calu3-24h-2
SARS2-ACE2-Ruxolitinib
SARS2-A549ACE2
SARS2-BALF
SARS1-MRC5-48h
MERS-Calu3-24h
SARS2-LungBiopsy
SARS2-Calu3-24h
SARS1-Calu3-24h
SARS2-Calu3-12h
SARS1-Calu3-12h
SARS2-PBMC
SARS2-Calu3-24h-2
SARS1-Calu3-0h
SARS2-A549
SARS2-Calu3-4h
SARS1-Calu3-4h
SARS2-NHBE
SARS1-Calu3-3h
SARS1-Calu3-12h-2
MERS-Calu3-12h
SARS1-Calu3-7h
MERS-Calu3-7h
ANTIGEN PRESENTATION
B CELLS
CELL CYCLE
DC ACTIVATION
ECM AND MIGRATION
INFLAMMATORY/TLR/CHEMOKINES
INTERFERON/ANTIVIRAL SENSING
MONOCYTES
NEUTROPHILS
NK CELLS
OTHERS
PLASMA CELLS
SIGNAL TRANSDUCTION
T CELLS
Negative log of P-values
0 1 2 3 4

Figure 6. Heatmap of negative log p-values of the differentially enriched modules of all the samples used in this meta-analysis study. High level annotation of each module (row) is represented by the classification assigned by Kazmin et al. (2017) based on pathways or cell lineage each module represents.

The Calu-3 cell line closely resembles the host transcriptional response. It is important to identify cell lines that resemble the host response upon infection. Visualization of log transformed scaled expression of some of the differentially expressed genes of the lung biopsy samples of COVID-19 patients and cell lines infected by SARS-CoV-2 (supplementary figure 2) demonstrates that Calu-3, an epithelial human lung cancer cell line, more accurately resembles the host immune response to SARS-CoV-2 infection than other cell lines such as A549 and NHBE (Blanco-Melo et al. 2020). Comparison of the enriched modules of various cell lines and clinical samples show that Calu-3 closely mirrors the host transcriptional response, i.e., similar to the clinical samples (figure 6) indicating this cell line's greater suitability for SARS-CoV-2 experimental studies.

Delayed/altered immune response of COVID-19 patients. Differences in the transcriptional immune response of SARS-CoV-2 patient derived samples provide insights into how the virus evades host immune responses. Comparison of the significantly enriched modules of the interferon and antiviral signaling group indicate that there is a lack of type I interferon response (M127) in PBMC samples as previously reported (Hadjadj et al. 2020) and also in BALF samples. Lung samples (and cell lines infected in vitro with any of three coronaviruses analysed here) have a profound representation of this module (figure 7) and other modules (M111.1, M111.0, M150, M13, M75) of this group demonstrating a strong interferon response in patients with severe disease and infected cell lines. Visualization of the scaled expression of the differentially expressed member genes of type I interferon response module of SARS-CoV-2 samples (supplementary figure 4) demonstrate that except for TAP1 gene (transporter associated with antigen processing 1, the gene-product of which is associated with antigen presentation by MHC class I), all of the member genes are strongly upregulated in lung biopsy samples. Several viruses are known to evade immune system detection by expressing proteins that have a direct effect on the expression of TAP1, hampering detection of infected cells (Zeidler et al. 1997). Strikingly, irrespective of viral load, younger individuals (<=30 group) have upregulated enrichment of type I interferon response (M127) module upon SARS-CoV-2 infection (figure 8), while the other groups (31-60 and >60 with medium and high viral load, 31-60 with low viral load) lack differential enrichment of this module, demonstrating altered immune response of these older individuals.

Silencing of RIG-I pathway by SARS-CoV-2 to evade detection by the host immune system. RIG-I-like receptor signaling (M68) module includes genes that influence antiviral immunity by playing a key role in pathogen sensing. These pathways are not enriched in any of the SARS-CoV-2 patient samples (or infected cell lines) (figure 7). In addition, in lung biopsy samples, interferon alpha response I module (M158.0 -- genes unique to this module are COL8A1, FGF5, IMPG2, ITGB4, LAMC2, MMP12, SFN, ST14, TNR) is downregulated while interferon alpha response II module (M158.1 -- genes unique to this module are FAM123A, IFNA2, IFNA21, IFNA5, IFNA8, PRL) is upregulated. Irrespective of the viral load (low, med, high) and the age groups (<=30, 31-60 and >60), none of the samples in the surveillance data (see supplementary table 1) have M68, M158.0 or M158.1 modules enriched, demonstrating lack of interferon alpha response and inactivation/silencing of RIG-I-like receptor signaling in

SARS-CoV-2 infected individuals. RIG-I-like receptors (RLRs) are expressed in various tissues and coordinate the induction of type I interferons (IFNs) (Loo et al. 2011) upon infection and act as the first line of defense against viral pathogens. TRIM25, an IFN inducible gene is known to mediate ubiquitylation of RIG-I (also known as DDX58), forming a complex that promotes interferon induction (Liu et al. 2016; Ozato et al. 2008; Gack et al. 2007). Visualization of the log transformed fold changes of the member genes of M158.0, M158.1 and M68 modules along with ZAP (also known as ZC3HAV1) (supplementary figure 5) in all SARS-CoV-2 samples shows that as a consequence of infection there is a profound upregulation of interferon alpha genes, no change in the expression of TRIM25, and a striking downregulation of SFN (also known as stratifin, 14-3-3ε) in the lung biopsy samples. SFN belonging to M158.0 (interferon alpha response I module) is known to be a binding factor of RIG-I and is essential for the stable interaction between TRIM25 and RIG-I, promoting ubiquitylation and thereby facilitating interferon induction (Liu et al. 2012).

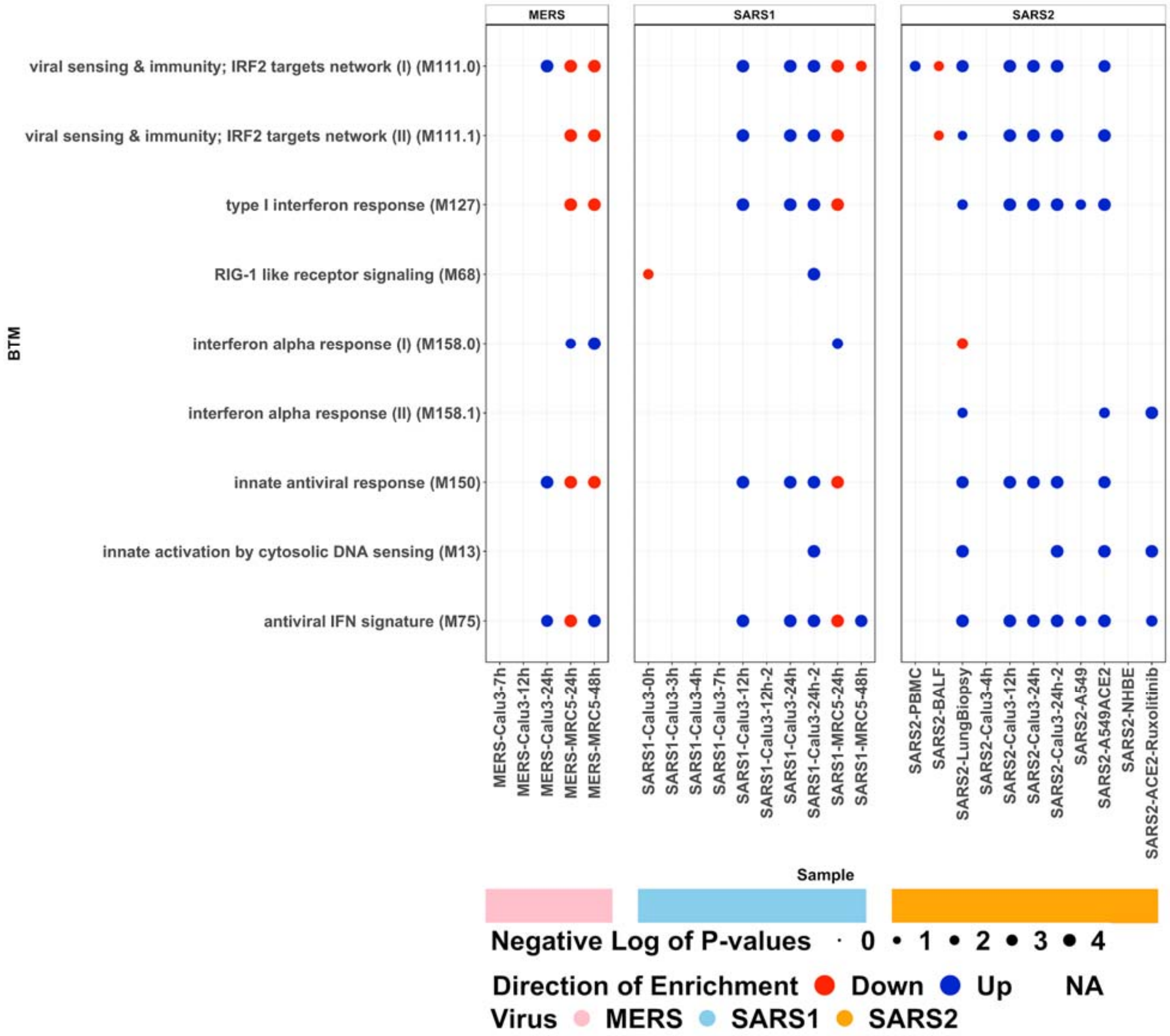

Figure 7. Plot showing -log10(p-values) of differentially enriched interferon and antiviral sensing modules (y-axis), colour of the circles corresponds to the direction of enrichment as indicated by mroast R package.

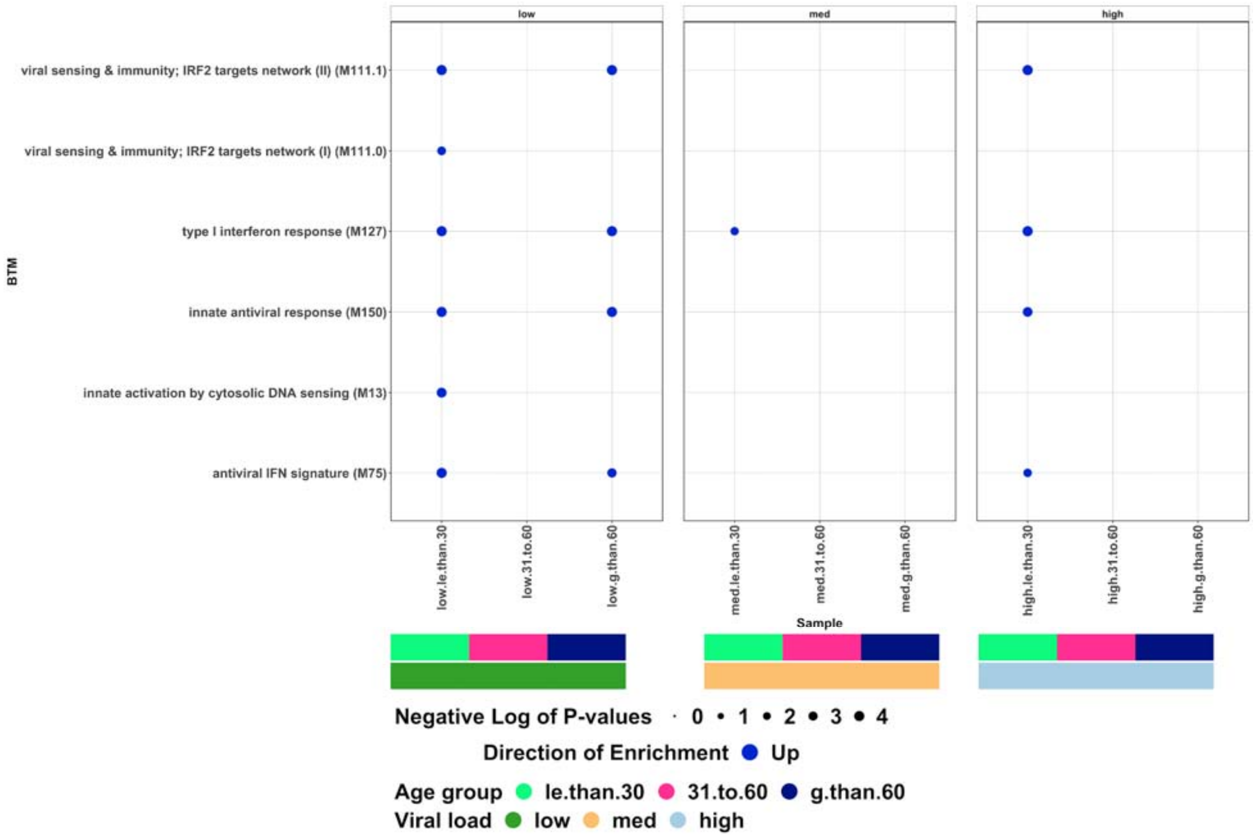

Figure 8. Plot showing -log10(p-values) of differentially enriched interferon and antiviral sensing modules (y-axis) of the surveillance data (Lieberman et al. 2020) stratified by age and viral load, colour of the circles corresponds to the direction of enrichment as indicated by mroast R package.

Ingenuity pathway analysis of the differentially expressed genes confirms there is a distinct immune pathway regulation profile for each of the SARS-CoV-2 clinical samples (supplementary figure 6) and no enrichment of the RIG-I signaling pathway in any of them. Viruses have evolved to develop refined mechanisms to counteract host immune responses. Many viruses are known to suppress host interferon response by antagonizing RIG-I signaling pathways, by manipulating the signaling cascades that led to suppression of type I interferons (Liu et al. 2016) and it is known SARS-CoV-1 and MERS-CoV downregulates RIG-I ubiquitylation through their viral deubiquitinating enzymes (Liu et al. 2016).

Gene co-expression analysis by WGCNA. To elucidate transcriptional response of the host in an unbiased way, weighted gene co-expression network analysis (WGCNA, see methods) was used to construct co-expression networks focussing on the correlated gene expression of the batch corrected surveillance data from Lieberman et al. (2020). WGCNA extracts modules of interest by identifying correlation-based interaction between genes and associates module ‘eigengenes’ with meta-data information such as gender and viral load, where an eigengene is a representative summary of the expression profile of each module from the first principal component of the standardized expression profile. WGCNA was separately applied to groups of samples belonging to the same age groups and infection status (Table 2).

Table 2. Table showing infection status, age group, number of samples in each age group, number of identified modules with the range of numbers of genes in each group

Sample (Infection status and age group)	Number of samples	Number of modules	Range (Min - Max)
neg <=30	16	36	59 - 474
neg 31-60	24	9	116 - 514
neg >60	14	29	59 - 533
pos <=30	52	3	432 - 653
pos 31-60	194	8	95 - 1697
pos >60	167	3	231 - 3015

Co-expression analyses identified three modules in SARS-CoV-2 positive individuals aged <=30, interestingly none of the modules are correlated with viral load or gender demonstrating a relatively controlled host immune response triggered by the virus in younger individuals (figure 9, functional annotation of modules by GSEA explained later in this paragraph). While eight modules are identified in SARS-CoV-2 positive individuals aged between 31-60, two of which are strongly positively correlated with high viral load and are strongly negatively correlated with low viral load (figure 9), three modules, in which two are positively correlated with high viral load and negatively correlated with low viral load are identified in infected individuals aged >60. Note, information about the infection status and age group is incorporated into the names of each module in order to avoid similarly named modules across sample groups. Gene set enrichment analysis with BTMs as reference modules performed with GeneOverlap package in R was used to identify the functional role of each identified module in all the groups. Within each age group, multiple assignments to the same reference module are aggregated by taking the maximum negative log of p-value from GeneOverlap package and significant enrichments grouped by their annotations are shown in figure 10.

Among all age groups (<=30, 31-60 and >60), relative to their negative counterparts, older individuals (>60) have the strongest host response upon infection, i.e., highest levels of perturbation/inflammation - strong up-regulation or down-regulation of the enriched modules. Cell cycle related modules in older SARS-CoV-2 (>60) infected individuals with lower viral load are disrupted (figure 9), possibly due to the cell cycle arrest mechanisms, which coronaviruses are known to activate for promoting viral replication (Dove et al. 2006). Another striking class of modules hyper-enriched in the older individuals (>60) are the monocyte related modules (figure 10) that contribute both to the innate and adaptive immunity of the host. We speculate that this enrichment, again possibly associated with the aging process, could be contributing to the dysregulated immune response in older patients. Due to the lack of recorded disease characteristics for these surveillance samples (Lieberman et al. 2020), we are unable to further associate the enrichment of these pathways with disease outcomes.

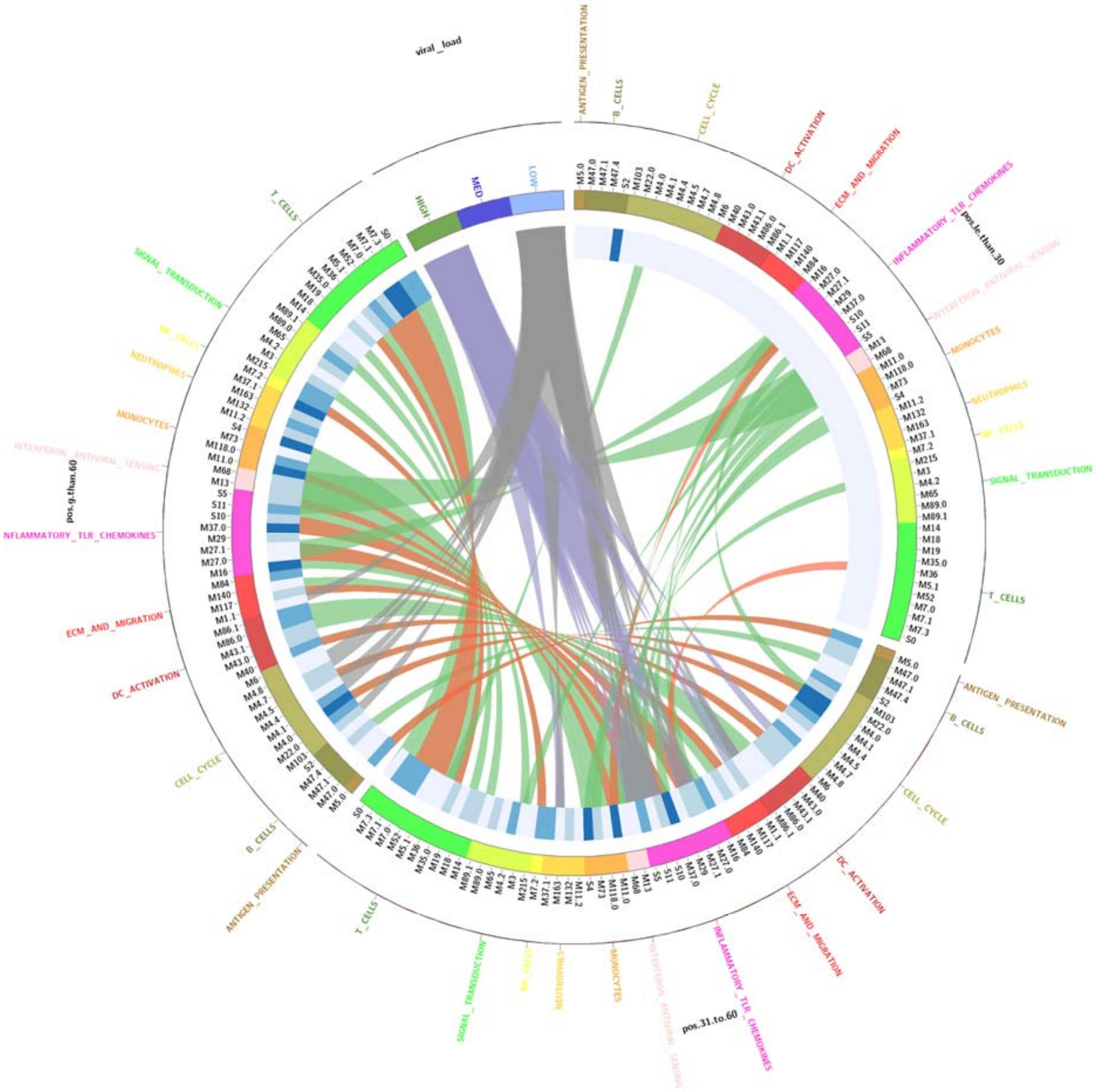

Figure 9. Circos plot showing enrichment of modules in the surveillance data (Lieberman et al. 2020) stratified by age groups (<=30, 31-60 and >60, denoted by outer black lines), a heatmap (blue scale) representing the negative log of p-values of enriched modules. Concordant modules (see methods) shared between age groups are linked by green ribbons and discordant modules by red ribbons. Significant (p<0.05) positively (r >= 0.3) and negatively (r <= -0.3) correlated modules with viral load are shown in purple and grey links, respectively.

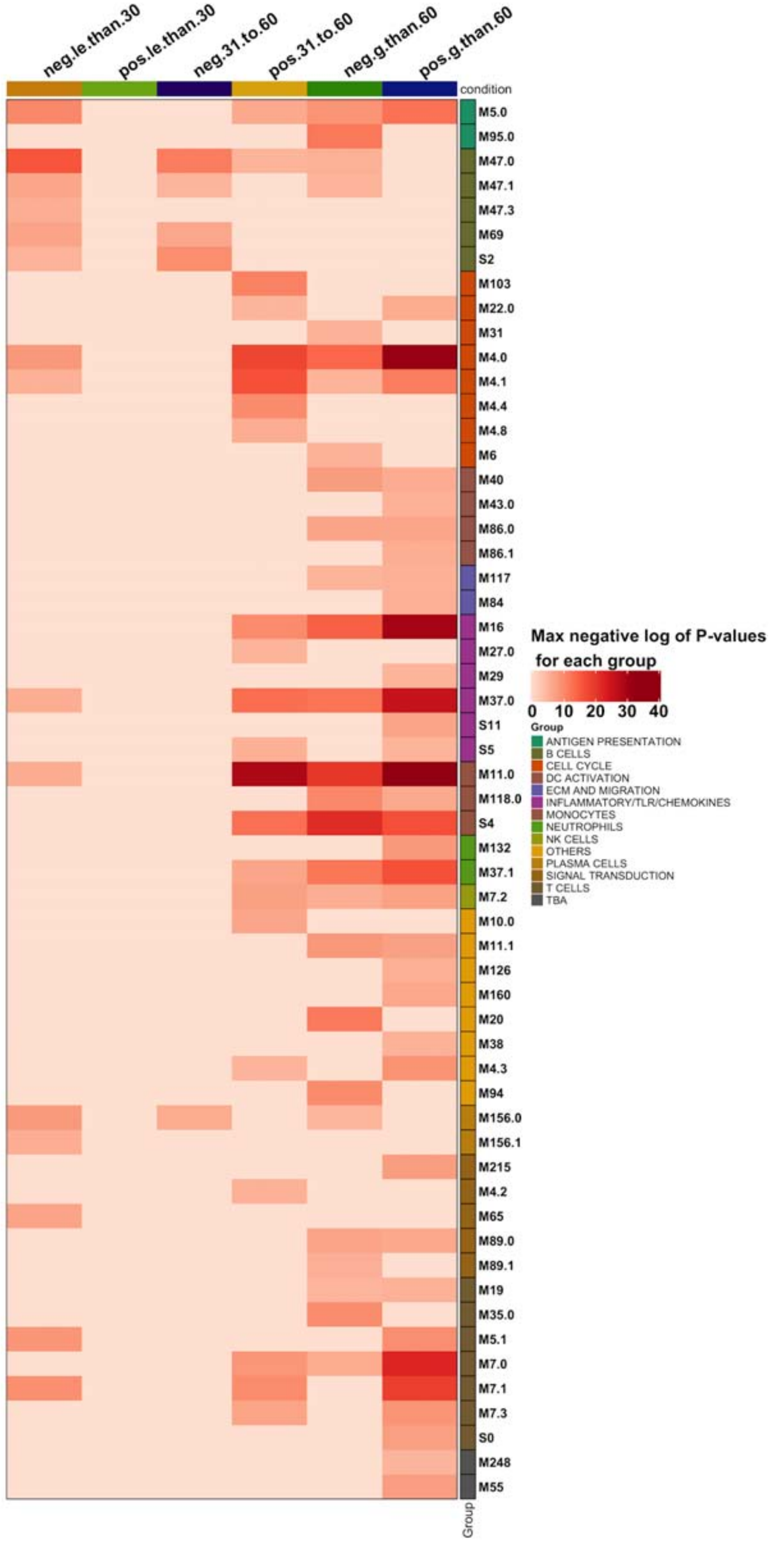

Figure 10. Heatmap of negative log of p-values less than 10^-5 of the WGCNA identified modules, functionally characterized by GeneOverlap package using BTMs as reference modules. High level annotation of each module (row) is represented by the classification assigned by Kazmin et al. 2017 based on pathways or cell lineage each module represents.

None of the B cell modules are significantly enriched in any of the age groups, possibly corresponding to the evasion mechanisms the virus uses in order to escape host mechanisms.

As expected, inflammatory, TLR and chemokine related modules are hyper-enriched in older patients (>60) in comparison to the samples from the 31-60 age group. Interestingly some of the modules are strongly enriched even in the negative older individuals (>60), possibly correlated to aging or underlying disease responses. It will be interesting to analyse how the enrichment of these modules accounts for the clinical characteristics of the disease and association with comorbidities.

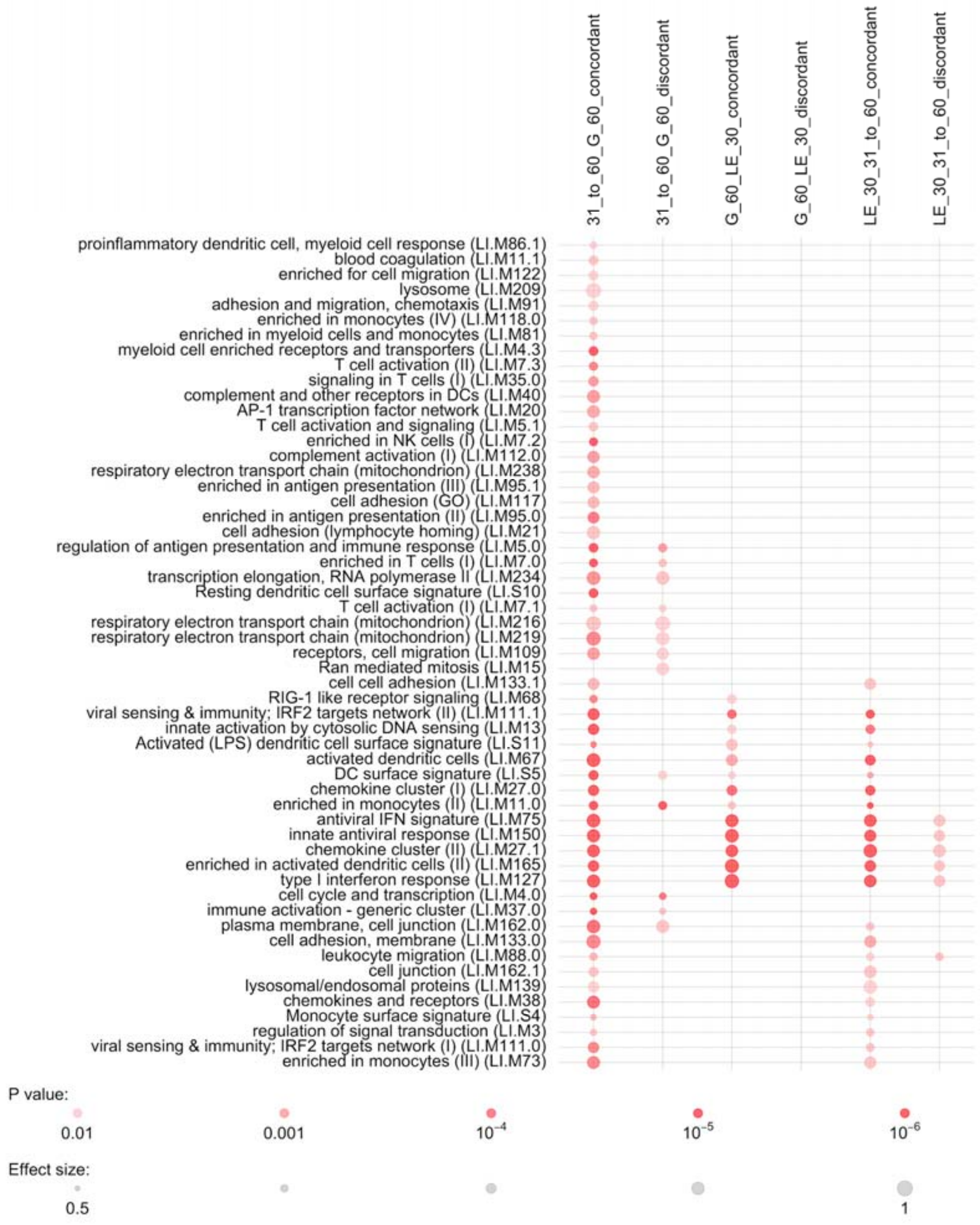

Figure 11. Dotplot of p-values of concordant and discordantly enriched modules identified by the tmod package in R, based on the disco score of the differential co-expressed member genes of WGCNA modules.

Performing enrichment analysis with tmod (see methods) confirms most of the enriched modules are consistent in the age groups 31-60 and >60. Discordant modules between these groups include antigen presentation and dendritic cell related modules, leading to differential enrichment of T cell activation and immune activation related modules. In line with the results of WGCNA analysis, tmod analysis shows that the cell cycle and transcription related modules are in discordance between the age groups 31-60 and >60. Type I interferon response and other antiviral response modules are concordant among the three groups, while some of the samples in the 31-60 group have these modules differentially enriched in comparison to the <=30 group and >60 groups (figure 11). These observations highlight the importance of age as a determining factor of altering viral inducible immune activation pathway mechanisms that lead to immune dysregulation in infected older individuals.

Decrease in oxidative phosphorylation (OxPhos) activity

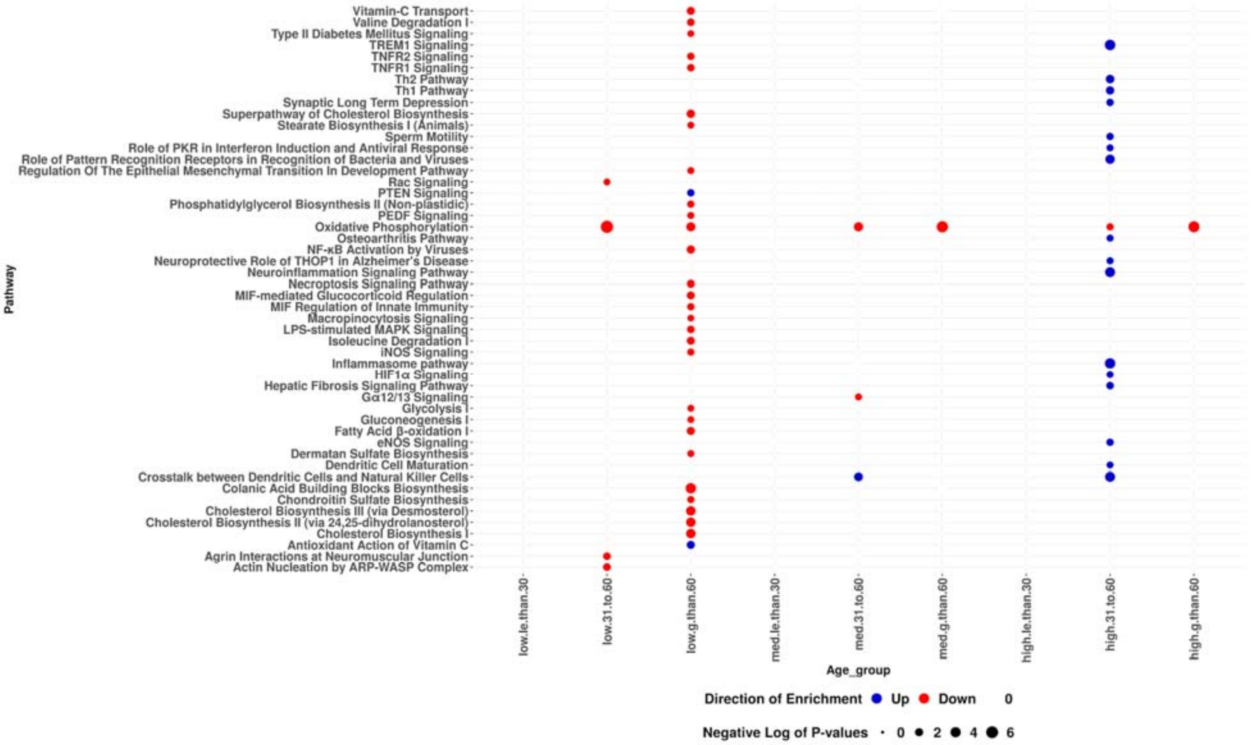

Figure 12. Dotplot of p-values of dysregulated pathways identified by IPA, based on the differential co-expressed member genes of WGCNA modules, colour corresponds to the direction of enrichment as inferred by IPA z-score.

To characterize immune response differences between age groups based on the viral load, we extracted differential expression information of the member genes of identified WGCNA modules from the results of limma-voom workflow (see materials and methods section) and used IPA to identify dysregulated pathways and their activation statuses. IPA infers activation status of pathways by calculating z-scores based on the differential regulation of genes and the direction of the effect associated with edges of experimentally observed molecular networks. Irrespective of the viral load, infected individuals in the age groups 31-60 and >60 have a decreased activity of oxidative phosphorylation pathway (figure 12) and altered regulation of mitochondrial dysfunction (supplementary figure 7) as inferred by IPA. Oxidative phosphorylation (OxPhos), a functional unit of mitochondria plays an important role in ATP (adenosine 5 -triphosphate) synthesis and apoptosis; any reduction in OxPhos activity leads to dysregulated mitochondrial ROS (reactive oxygen species) signaling, reduced cellular ATP and trigger ROS-mediated cell damages (Fekete et al. 2018; Yoshizumi et al. 2017). Recovery of OxPhos activity re-establishes RIG-I-like receptor (RLR) mediated signal transduction counteracting impaired induction of interferons in viral infected cells (Yoshizumi et al. 2017), indicating OxPhos activity could be an important requirement for RLR-mediated signaling transduction. We hypothesize that SARS-CoV-2 suppresses RIG-I mediated antiviral innate immunity by impairing oxidative phosphorylation activity of the host.

Discussion

The severity of COVID-19 is due to differences in host immune responses to SARS-CoV-2 that are strongly associated with genetic factors, age and specific comorbidities. Understanding mechanistically how SARS-CoV-2 perturbs and evades the immune system provides much needed insights into viral escape mechanisms, immunopathology and directions for the development of novel therapeutics. In this study, we use a meta-analysis approach to compare enriched gene sets/functional modules in transcriptomics datasets, combined with a network approach, to identify distinct transcriptional profile signatures exhibited by SARS-CoV-2 infected patient samples and cell lines (figure 13). We used a well-defined functional blood transcriptomics module set that integrates data obtained from more than 500 transcriptomics studies and various sources (Li et al. 2014). These modules have more discriminative power in identifying context-specific gene modules than results arising from individual experiments, and are being increasingly used as a data-rich context in transcriptomics studies. We also used Ingenuity pathway analysis software to identify pathways that are dysregulated upon SARS-CoV-2 infection in patient and cell line samples.

Contrary to expectation, our comparison of SARS-CoV-2 infected cell lines and patient derived samples collected with published SARS-CoV-1 and MERS-CoV datasets, showed that host responses to SARS-CoV-2 are less similar to those against SARS-CoV-1 than the latter are to responses to MERS-CoV (figure 13). SARS-CoV-1 and MERS-CoV elicit differential regulation of genes responsible for important immune functions such as adaptive immunity, cell cycle damage, inflammation and innate immunity, while in COVID-19 patients and SARS-CoV-2 infected cell lines, some of these crucial signaling pathways are being repressed (Blanco-Melo et al. 2020).

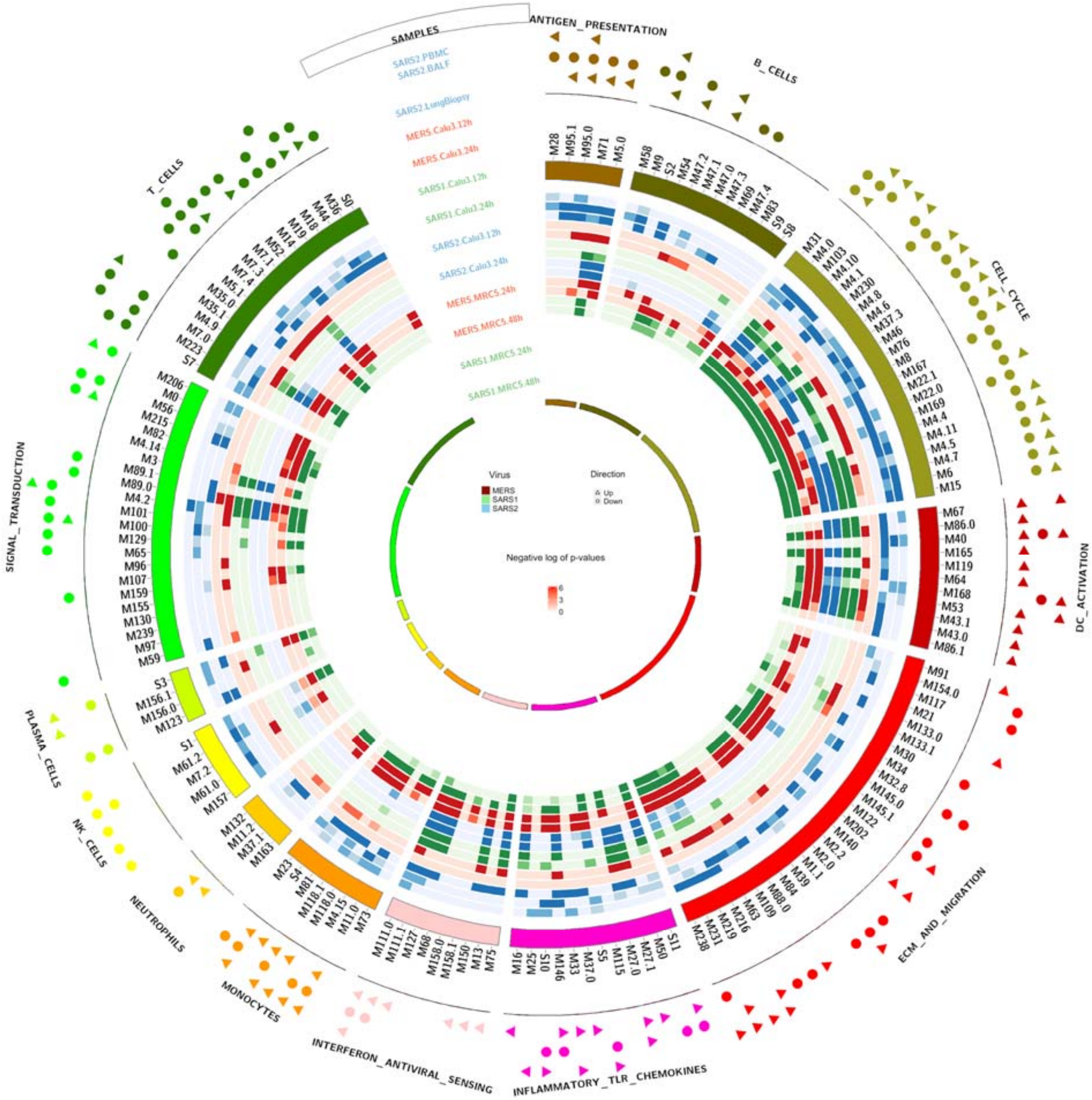

Figure 13. Circos plot showing enrichment of modules in SARS-CoV-2 clinical samples and SARS-CoV-2, SARS-CoV-1 and MERS-CoV infected cell lines. Each circle represents the negative log of p-values of enriched modules in each sample, coloured by virus (see 'samples' legend at 11 o'clock). The 3 outer circles represent the direction of enrichment of modules of the clinical samples of SARS-CoV-2 (PBMC, BALF and lung samples) as predicted by MROAST, a circle representing down-regulation and an arrow indicating up-regulation of the modules.

Our analysis indicates SARS-CoV-2 evades innate immunity by not triggering RIG-I signaling pathway, thereby delaying the type-I interferon response. The RIG-I signaling pathway is known to be interfered with by the nucleocapsid protein in both SARS-CoV-1 and MERS-CoV, through interaction of N protein with TRIM25 thereby inhibiting TRIM25-mediated RIG-I ubiquitination and suppressing type I IFN production (Hu et al. 2017). In SARS-CoV-1, increased infection dose has been shown to enhance suppression of RIG-I signaling (Hu et al. 2017) and delayed ISG expression combined with immune dysregulation has been shown (Channappanavar et al.

2016) to be a contributor to disease severity in mice, indicating the role of innate immunity in control of infection and how in older individuals can lead to severe disease. Unlike SARS-CoV-1, avoidance/delaying of type-I interferon response in SARS-CoV-2 infection is probably linked to CpG depletion and ZAP-TRIM25 evasion (Li et al. 2017). Zinc finger antiviral protein (ZAP, also known as ZC3HAV1) acts against RNA viruses by detecting viral RNAs that have a higher CpG dinucleotide frequencies than the host mRNAs. TRIM25 interacts with ZAP through its SPRY domain and enhances its ability to inhibit translation of the viral genomes. The shorter isoform of ZAP, ZAPS associates with RIG-I and functions as a stimulator of interferon responses during viral infections (Hayakawa et al. 2011). Detection of the viral genes by ZAP, which in turn depends on the CpG frequencies of the viral mRNA, is crucial for the activation of RIG-I signaling pathway and induction of interferon alpha responses. We are unable to determine from the available data if the avoidance of RIG-I signaling is a determinant of disease severity in COVID-19 patients. Possibly the infection dose accounts for severity of illness: older/co-morbid patients having their interferon alpha pathway evaded for longer due to (relatively) lower virus dose, with younger-severe cases due to a higher dose-effect. A recent study has demonstrated that the nonstructural protein 1 (NSP1) of SARS-CoV-2 blocks RIG-I dependent immune responses (Thoms et al. 2020), while another showed that ZAP restricts SARS-CoV-2 and its knock down in Calu-3 cells enhanced viral replication particularly upon treatment with IFN-α or IFN-γ (Nchioua et al. 2020).

The susceptibility of SARS-CoV-2 to IFN-I has been tested by pretreating Vero E6 cells with IFN-α (Lokugamage et al. 2020) resulting in a significant reduction in viral replication and reduced nucleocapsid protein production of SARS-CoV-2, while SARS-CoV-1 robustly expressed viral proteins in IFN-α treated cells after 48 hours. This sensitivity to interferon indicates immunotherapy that activates the RIG-I pathway may lead to restoration of early type I interferon response in patients, counteracting SARS-CoV-2 infection. A recent PRRs (pattern recognition receptor) stimulating study demonstrates the pathophysiological role of type III interferons in COVID-19 patients (Broggi et al. 2020). Collectively these results indicate immunopathology due to SARS-CoV-2 infection predominant in older people is driven by immune dysregulation, i.e., an inability to control disease. Regulation of interferon alpha response despite being a moderator of SARS-CoV-2 infection in cells will probably not work in older people due to immune dysregulation. A recent retrospective study shows administration of IFN in later stages of the disease to be associated with increased mortality and delayed recovery in COVID-19 patients (Wang et al. 2020), suggesting the timing of the therapy to be crucial for favorable clinical outcomes. Another interesting study compared type I interferon response in mild vs severe patients using single-cell transcriptomics data to determine its role in aggravating inflammation in COVID-19 patients (Lee et al. 2020).

What has become clear is pathology of SARS-CoV-2 infected individuals depends on many factors such as sex, age, genetics etc., with increasing age the most important determinant of the disease outcome in COVID-19 patients, with those 80 years or older having more than 20-fold risk of death than those aged between 50 to 59 (Williamson et al. 2020). Age-related changes in the host innate immune system such as declining activities of monocytes, macrophages and dendritic cells weaken the ability to respond to infections or gain protective immunity from vaccination and this immunosenescence impacts the adaptive immune response of the host (Panda et al. 2009). During inflammation or infection, monocytes are recruited through blood circulation, differentiate into antigen presenting cells and are then involved in resolving inflammation (Kratofil et al. 2017). Reduced expression of certain chemokine receptors like CX3CR1 due to aging, affects the ability of monocytes to migrate to the inflammatory sites to clear up inflammation and thus increased number of monocytes in older individuals is not necessarily positively correlated with increased functionality (Seidler et al. 2010). Our results demonstrate that the hyper-enrichment of monocyte related modules not only in SARS-CoV-2 infected older individuals but also in older negative controls may play an important role in immunopathology in the older individuals, possibly correlating with clinical outcomes (Pence 2020). A recent study (Giamarellos-Bourboulis et al. 2020) observed a sudden decrease in monocyte expression preceding respiratory failure in COVID-19 patients.

SARS-CoV-2 RNA genome is enriched in the host mitochondria and nucleolus and this localization is predicted to induce mitochondrial dysfunction, likely to increase viral replication without being detected by the host immune system (Singh et al. 2020). ORF9b of SARS-CoV-1 is known to influence innate immunity by localizing into host mitochondria and promoting viral replication (Shi et al. 2014). Several viruses are known to modulate mitochondria-mediated antiviral immunity and possess strategies either to hijack host mitochondrial proteins or to mimic them (Anand and Tikoo 2013). In this study, we show that SARS-CoV-2 infected individuals irrespective of age have their mitochondrial mechanisms altered by the virus leading to mitochondrial dysfunction. As oxidative phosphorylation generates energy important for viral replication, selective regulation of this activity by the viruses results in sustained viral replication (Cao et al. 2017) during host shutoff induced by viral infections. Early after infection, hepatitis C virus limits oxidative phosphorylation activity to efficiently allow for viral replication (Gerresheim et al. 2019) and several other viruses suppress immune responses by reprogramming OxPhos activity and other mitochondrial functions (Moreno-Altamirano et al. 2019), thereby manipulating type I interferon response of the host. RIG-I mediated antiviral responses are known to rely on oxidative phosphorylation activity to produce type I interferons (Yoshizumi et al. 2017; Fekete et al. 2018); mitochondrial DNA deficiency with abnormal OxPhos activity results in impairment of RLR-mediated antiviral signaling enhancing susceptibility of the host to viral infection (Yoshizumi et al. 2017). SARS-CoV-2 seems to down-regulate OxPhos activity that is crucial for early detection of the virus by the host innate immune system mechanisms, thus accelerating viral replication inside the host.

In conclusion, meta analysis of SARS-CoV-2 transcriptomic data sets coupled with gene set and network analysis had revealed that the virus establishes infection by delaying/avoidance of type-I interferon response by suppressing OxPhos dependent RIG-I signaling pathway, possibly by avoiding TRIM25-ZAP detection by the immune system of the host. Immunosenescence in older individuals exhibited by negative controls in the surveillance data reveals that the host factors such as age related immune dysregulation and co-morbidities play a crucial role in determining severity and outcome of the disease. This study demonstrates the ability of focused gene set and network analyses -- applied to transcriptomics datasets from various sources -- to provide valuable insights into the disease characteristics of COVID-19.

Materials and methods

The SARS-CoV-2 PBMC-BALF transcriptome patient dataset (Xiong et al. 2020) was downloaded from the Genome Sequence Archive (https://bigd.big.ac.cn/) using the accession number CRA002390. The paired end reads were mapped onto the human hg38 genome using the STAR aligner (Dobin et al. 2013). The resulting mapped reads were quantified using the featureCounts program (Liao et al. 2014) in the Subread R package (Liao et al. 2019). SARS-CoV-2 cell line and lung biopsy data (Blanco-Melo et al. 2020; Wyler et al. 2020), SARS-CoV-1 (Josset et al. 2013; Sims et al. 2013; Frieman et al. 2014) and MERS-CoV (Josset et al. 2013; Frieman et al. 2013) were downloaded from NCBI GEO using the following accession numbers: GSE147507, GSE45042, GSE33267, GSE56192, GSE148729. Where available, the mapped read count data was downloaded for each RNA-seq dataset and analysed. If mapped data was unavailable, the sequencing data was downloaded and processed as described above. Microarray data of SARS-CoV-1 and the MERS-CoV were processed using the GEOquery package (Davis and Meltzer 2007), implemented in the R statistical language. Differential expression and BTM enrichment analysis of all the datasets were performed with limma workflow (Ritchie et al. 2015), using a design model specifying sample types, time points wherever applicable, and infection status as covariates. As an additional preprocessing step, RNA-seq counts were scaled and normalized by the TMM (trimmed mean of M-values) method of edgeR package (Robinson et al. 2010) and log transformed using voom (Law et al. 2014), followed by differential expression analysis using the limma workflow.

Genes with an absolute log transformed expression ratio of ≥1, and with a Benjamini and Hochberg (BH) (Benjamini and Hochberg 1995) adjusted p-value of ≤0.01, were considered differentially expressed. The differential gene lists containing gene identifiers, log transformed fold change and their corresponding false discovery rates (FDR) were analysed with the Ingenuity Pathway Analysis (IPA) software (https://www.qiagenbioinformatics.com/products/ingenuity-pathway-analysis) and differentially regulated canonical pathways identified. Gene set testing using downloaded BTMs were performed using the MROAST package (Wu et al. 2010) with the same design model described above. For both the IPA and BTM enrichment analysis, p-value correction for multiple testing was using the BH method; those with an FDR of 5% were considered differentially regulated. Dysregulated canonical pathways and enriched BTMs were compared across all SARS-CoV-2 datasets, to differentiate host immune response in different samples upon infection, as well as to elucidate differences between patient samples and cell line responses. By comparing SARS-CoV-2 module enrichment with SARS-CoV-1 and MERS-CoV, differences in the overall response exhibited by these viruses in cell lines and distinct responses of the SARS-CoV-2 were identified.

Mapped read counts from a transcriptomic dataset of nasopharyngeal swabs comprising 430 SARS-CoV-2 positive and 54 negative samples (Lieberman et al. 2020), downloaded from NCBI GEO using the accession number GSE152075, were analyzed to understand the differences associated with age and viral load in SARS-CoV-2 infected individuals. We used the variancePartition package (Hoffman et al. 2016) in R to compute the fraction of variance explained by known biological and technical covariates such as sequencing batch and gender. Violin plots demonstrating known sources of variation in the data before and after correction are depicted in supplementary figure 8, showing the major technical driver of variation to be sequencing batch and biological variation to be viral load. We used the voom function in the limma R package to correct for batch and gender and retained the effect of viral load to stratify data.

Co-expression networks were constructed using the weighted gene correlation network analysis (Langfelder et al. 2008) in R. Based on the hierarchical clustering of the normalized expression of the genes, correlated networks of genes were identified among different age groups using a dynamic cuttree algorithm. The minimum module size was set to 50 and correlation of module eigengenes with viral load computed using pearson correlation analysis. To determine the functional roles of the constructed WGCNA modules, the Fisher exact test was used, implemented in the GeneOverlap package (Shen 2020), using BTMs as reference modules and enriched modules across age groups were compared. Concordance and discordance of module enrichment across age groups were determined by calculating the disco.score of the differential co-expressed member genes of WGCNA modules using the disco package (Domaszewska et al. 2017) in R. For each gene-pair, the degree of change in gene expression (log-fold change), statistical significance of the differential expression (p-values) and direction of differential expression are used to calculate the disco.score. Gene set enrichment analysis on decreasing and increasing ordered lists of genes based on the disco.score were used to identify concordant and discordant modules, respectively, across each pairwise age groups using the tmod package (Weiner et al. 2016) in R against the reference modules.

Table 1. Datasets used in the manuscript and images. Source and reference information is shown. More detailed information about the datasets can be found in supplementary table 1.

Sample	Virus	Reference
PBMC	SARS-CoV-2	Xiong et al. 2020
BALF	SARS-CoV-2	Xiong et al. 2020
Lung Biopsy	SARS-CoV-2	Blanco-Melo et al. 2020
Calu-3	a. SARS-CoV-2 b. SARS-CoV c. MERS-CoV	a. Blanco-Melo et al. 2020 b. Josset et al. 2013 Sims et al. 2013 c. Josset et al. 2013
A549	SARS-CoV-2	Blanco-Melo et al. 2020
A549-ACE2	SARS-CoV-2	Blanco-Melo et al. 2020
A549-ACE2-Ruxolitnib	SARS-CoV-2	Blanco-Melo et al. 2020
NHBE	SARS-CoV-2	Blanco-Melo et al. 2020
MRC5	a.SARS-CoV b.MERS-CoV	Frieman et al. 2014
Surveillance data	SARS-CoV-2	Lieberman et al. 2020

Acknowledgements

DR, MP, SK, SW and QG are funded by the MRC (MC_UU_1201412). We thank the data producers for sharing their data freely.

References

1. Anand, S. K. & Tikoo, S. K. Viruses as modulators of mitochondrial functions. Adv. Virol. 2013, (2013).
2. Barrett, T. et al. NCBI GEO: Archive for functional genomics data sets - Update. Nucleic Acids Res. 41, 991–995 (2013).
3. Bastard, P. et al. Auto-antibodies against type I IFNs in patients with life-threatening COVID-19. Science (370), eabd4585 (2020).
4. Bergmann, C. C., Tschen, S. I., Ramakrishna, C., Gonzales, J. M. & Stohlman, S. A. Coronavirus immunity: From T cells to B cells. Adv. Exp. Med. Biol. 581, 341–349 (2006).
5. Blanco-Melo, D. et al. Imbalanced Host Response to SARS-CoV-2 Drives Development of COVID-19. Cell 181, 1036-1045.e9 (2020).
6. Broggi, A. et al. Type III interferons disrupt the lung epithelial barrier upon viral recognition. Science (369), 706-712 (2020).
7. Cai, H. Sex difference and smoking predisposition in patients with COVID-19. Lancet Respir. Med. 8, e20 (2020).
8. Cao, S., Dhungel, P. & Yang, Z. Going against the Tide: Selective Cellular Protein Synthesis during Virally Induced Host Shutoff. J. Virol. 91, 1–5 (2017).
9. Channappanavar, R. et al. Dysregulated Type I Interferon and Inflammatory Monocyte-Macrophage Responses Cause Lethal Pneumonia in SARS-CoV-Infected Mice. Cell Host Microbe 19, 181–193 (2016).
10. Chen, Y., Zhou, Z. & Min, W. Mitochondria, oxidative stress and innate immunity. Front. Physiol. 9, 1–10 (2018).
11. Dobin, A. et al. STAR: Ultrafast universal RNA-seq aligner. Bioinformatics 29, 15–21 (2013).
12. Domaszewska, T. et al. Concordant and discordant gene expression patterns in mouse strains identify best-fit animal model for human tuberculosis. Sci. Rep. 7, 1–13 (2017).
13. Dove, B., Brooks, G., Bicknell, K., Wurm, T. & Hiscox, J. A. Cell Cycle Perturbations Induced by Infection with the Coronavirus Infectious Bronchitis Virus and Their Effect on Virus Replication. J. Virol. 80, 4147–4156 (2006).
14. Fekete, T. et al. Human Plasmacytoid and Monocyte-Derived Dendritic Cells Display Distinct Metabolic Profile Upon RIG-I Activation. Front. Immunol. 9, 3070 (2018).
15. Fortin, C. F., Lesur, O. & Fulop, T. Effects of aging on triggering receptor expressed on myeloid cells (TREM)-1-induced PMN functions. FEBS Lett. 581, 1173–1178 (2007).
16. Frieman M, Coleman C, Daugherty SC, Rasko D, Shefchek K, Sengamalay N, Tallon LJ, Sadzewicz L, F. C. Transcriptomic analysis of the Novel Middle East Respiratory Syndrome Coronavirus (MERS-CoV).
17. Gack, M. U. et al. TRIM25 RING-finger E3 ubiquitin ligase is essential for RIG-I-mediated

antiviral activity. Nature 446, 916–920 (2007).

18. Gerresheim, G. K., Roeb, E., Michel, A. M. & Niepmann, M. Oxidative Phosphorylation , Reminiscent of the Warburg Effect in Cancer Cells. Cells 8, 1410 (2019).
19. Giamarellos-Bourboulis, E. J. et al. Complex Immune Dysregulation in COVID-19 Patients with Severe Respiratory Failure. Cell Host & Microbe 27, 992-1000 (2020).
20. Gu, Z., Eils, R. & Schlesner, M. Complex heatmaps reveal patterns and correlations in multidimensional genomic data. Bioinformatics 32, 2847–2849 (2016).
21. Haagmans, B. L. et al. Pegylated interferon-α protects type 1 pneumocytes against SARS coronavirus infection in macaques. Nat. Med. 10, 290–293 (2004).
22. Hadjadj, J., Yatim, N., Barnabei, L., Corneau, A. & Boussier, J. Impaired type I interferon activity and inflammatory responses in severe COVID-19 patients. Science (369), 718–724 (2020).
23. Hayakawa, S. et al. ZAPS is a potent stimulator of signaling mediated by the RNA helicase RIG-I during antiviral responses. Nat. Immunol. 12, 37–44 (2011).
24. Hochberg, Y. Controlling the False Discovery Rate□: A Practical and Powerful Approach to Multiple Testing Author (s): Yoav Benjamini and Yosef Hochberg Source□: Journal of the Royal Statistical Society . Series B (Methodological), Vol . 57 , No . 1 (1995), Publi. 57, 289–300 (2016).
25. Hoffman, G. E. & Schadt, E. E. variancePartition: Interpreting drivers of variation in complex gene expression studies. BMC Bioinformatics 17, 483 (2016).
26. https://www.qiagenbioinformatics.com/products/ingenuity-pathway-analysis. IPA.
27. Hu Y, Wei Li, Ting Gao, Yan Cui, Yanwen Jin, Ping Li, Qingjun Ma, Xuan Liu, Cao C. The Severe Acute Respiratory Syndrome Coronavirus Nucleocapsid Inhibits Type I Interferon Production by Interfering with TRIM25-Mediated RIG-I Ubiquitination. J Virol 91, e02143-16 (2017).
28. Huang C, Yeming Wang, Xingwang Li, Lili Ren, Jianping Zhao, Yi Hu, Li Zhang, Guohui Fan, Jiuyang Xu, Xiaoying Gu, Zhenshun Cheng, Ting Yu, Jiaan Xia, Yuan Wei, Wenjuan Wu, Xuelei Xie, Wen Yin, Hui Li, Min Liu, Yan Xiao, Hong Gao, Li Guo, Junga, B. C. Clinical features of patients infected with 2019 novel coronavirus in Wuhan, China. Lancet 395, 497–506 (2020).
29. Hüttemann, M., Lee, I., Samavati, L., Yu, H. & Doan, J. W. Regulation of mitochondrial oxidative phosphorylation through cell signaling. Biochim. Biophys. Acta - Mol. Cell Res. 1773, 1701–1720 (2007).
30. Ingenuity Systems. Ingenuity Downstream Effects Analysis in IPA. 1–5 (2011).
31. Josset, L. et al. Cell host response to infection with novel human coronavirus EMC predicts potential antivirals and important differences with SARS coronavirus. MBio 4, 1–11 (2013).
32. Kazmin, D. et al. Systems analysis of protective immune responses to RTS,S malaria vaccination in humans. Proc. Natl. Acad. Sci. U. S. A. 114, 2425–2430 (2017).

33. Kim, D. et al. The Architecture of SARS-CoV-2 Transcriptome. Cell 181, 914-921 (2020).
34. Kratofil, R. M., Kubes, P. & Deniset, J. F. Monocyte conversion during inflammation and injury. Arterioscler. Thromb. Vasc. Biol. 37, 35–42 (2017).
35. Langfelder, P. & Horvath, S. WGCNA: An R package for weighted correlation network analysis. BMC Bioinformatics 9, (2008).
36. Law, C. W., Chen, Y., Shi, W. & Smyth, G. K. Voom: Precision weights unlock linear model analysis tools for RNA-seq read counts. Genome Biol. 15, 1–17 (2014).
37. Lee, J. S. et al. Immunophenotyping of COVID-19 and influenza highlights the role of type I interferons in development of severe COVID-19. Sci. Immunol. 5, 1–17 (2020).
38. Li S, Nadine Rouphael, Sai Duraisingham, Sandra Romero-Steiner, Scott Presnell, Carl Davis, Daniel S Schmidt, Scott E Johnson, Andrea Milton, Gowrisankar Rajam, Sudhir Kasturi, George M Carlone, Charlie Quinn, Damien Chaussabel, A Karolina Palucka, B. P. Molecular signatures of antibody responses derived from a systems biological study of 5 human vaccines. Nat Immunol 15, 195–204 (2014).
39. Li, M. M. H. et al. TRIM25 Enhances the Antiviral Action of Zinc-Finger Antiviral Protein (ZAP). PLoS Pathog. 13, 1–25 (2017).
40. Li, S., Todor, A. & Luo, R. Blood transcriptomics and metabolomics for personalized medicine. *Comput. Struct. Biotechnol. J.* **14**, 1–7 (2016).
41. Liang, Y. et al. Highlight of Immune Pathogenic Response and Hematopathologic Effect in SARS-CoV, MERS-CoV, and SARS-Cov-2 Infection. Front. Immunol. 11, 1–11 (2020).
42. Liao, Y., Smyth, G. K. & Shi, W. The R package Rsubread is easier, faster, cheaper and better for alignment and quantification of RNA sequencing reads. Nucleic Acids Res. 47, (2019).
43. Liao, Y., Smyth, G. K. & Shi, W. FeatureCounts: An efficient general purpose program for assigning sequence reads to genomic features. Bioinformatics 30, 923–930 (2014).
44. Lieberman, N. A. P. et al. In vivo antiviral host transcriptional response to SARS-CoV-2 by viral load, sex, and age. PLoS Biol. 18, e3000849 (2020).
45. Liu, H. M. et al. The mitochondrial targeting chaperone 14-3-3ε regulates a RIG-I translocon that mediates membrane association and innate antiviral immunity. Cell Host Microbe 11, 528–537 (2012).
46. Liu, S. Y., Sanchez, D. J., Aliyari, R., Lu, S. & Cheng, G. Systematic identification of type I and type II interferon-induced antiviral factors. Proc. Natl. Acad. Sci. U. S. A. 109, 4239–4244 (2012).
47. Liu, Y., Olagnier, D. & Lin, R. Host and viral modulation of RIG-I-mediated antiviral immunity. Front. Immunol. 7, 1–12 (2017).
48. Lokugamage K. G, Adam Hage, Craig Schindewolf, Ricardo Rajsbaum, V. D. M. SARS-CoV-2 is sensitive to type I interferon pretreatment. (2020).

49. Loo, Y. M. & Gale, M. Immune Signaling by RIG-I-like Receptors. Immunity 34, 680–692 (2011).
50. Lukacs-Kornek, V., Engel, D., Tacke, F. & Kurts, C. The role of chemokines and their receptors in dendritic cell biology. Front. Biosci. 13, 2238–2252 (2008).
51. Mehta, P. et al. COVID-19: consider cytokine storm syndromes and immunosuppression. Lancet 395, 1033–1034 (2020).
52. Moreno-Altamirano, M. M. B., Kolstoe, S. E. & Sánchez-García, F. J. Virus control of cell metabolism for replication and evasion of host immune responses. Front. Cell. Infect. Microbiol. 9, 1–15 (2019).
53. Nchioua R , Dorota Kmiec , Janis Müller , Carina Conzelmann, Rüdiger Groß, Chad Swanson , Stuart Neil , Steffen Stenger , Daniel Sauter, Jan Münch, K. M. J. S. & Kirchhoff, F. The Zinc Finger Antiviral Protein restricts SARS-CoV-2. (2020).
54. Neufeldt, C. J. et al. SARS-CoV-2 infection induces a pro-inflammatory cytokine response through cGAS- STING and NF-□B. (2020).
55. Ozato K, Dong-Mi Shin, Tsung-Hsien Chang, and Herbert C. M. III. TRIM family proteins and their emerging roles in innate immunity. Nat Rev Immunol. 8, 849–860 (2008).
56. Pairo-Castineira, E. et al. Genetic mechanisms of critical illness in Covid-19. medRxiv (2020).
57. Panda A, Alvaro Arjona, Elizabeth Sapey, Fengwei Bai, Erol Fikrig, Ruth R. Montgomery, Janet M. Lord, and A. C. S. Human innate Immunosenescence: causes and consequences for immunity in old age. Trends Immunol 30, 325–333 (2009).
58. Pence, B. D. Severe COVID-19 and aging: are monocytes the key? GeroScience 42, 1051–1061 (2020).
59. Pinto, B. G. et al. ACE2 Expression is Increased in the Lungs of Patients with Comorbidities Associated with Severe COVID-19. medRxiv doi:10.1101/2020.03.21.20040261 (2020).
60. R Core Team. R: A Language and Environment for Statistical Computing. (2019).
61. Ritchie, M. E. et al. Limma powers differential expression analyses for RNA-sequencing and microarray studies. Nucleic Acids Res. 43, e47 (2015).
62. Robinson, M. D., McCarthy, D. J. & Smyth, G. K. edgeR: A Bioconductor package for differential expression analysis of digital gene expression data. Bioinformatics 26, 139–140 (2009).
63. Roe, K., Gibot, S. & Verma, S. Triggering receptor expressed on myeloid cells-1 (TREM-1): A new player in antiviral immunity? Front. Microbiol. 5, 1–11 (2014).
64. Sean, D. & Meltzer, P. S. GEOquery: A bridge between the Gene Expression Omnibus (GEO) and BioConductor. Bioinformatics 23, 1846–1847 (2007).
65. Shen L, S. M. GeneOverlap: Test and visualize gene overlaps. R package version 1.24.0. 2020.
66. Shi, C.-S. et al. SARS-Coronavirus Open Reading Frame-9b Suppresses Innate Immunity by Targeting Mitochondria and the MAVS/TRAF3/TRAF6 Signalosome. J. Immunol. 193, 3080–3089 (2014).

67. Sims, A. C. et al. Release of Severe Acute Respiratory Syndrome Coronavirus Nuclear Import Block Enhances Host Transcription in Human Lung Cells. J. Virol. 87, 3885–3902 (2013).
68. Singh, K. K., Chaubey, G., Chen, J. Y. & Suravajhala, P. Decoding SARS-CoV-2 hijacking of host mitochondria in covid-19 pathogenesis. Am. J. Physiol Cell Physiol. 319, C258–C267 (2020).
69. Subramanian, A. et al. Gene set enrichment analysis: A knowledge-based approach for interpreting genome-wide expression profiles. Proc. Natl. Acad. Sci. U. S. A. 102, 15545–15550 (2005).
70. Tay, M. Z., Poh, C. M., Rénia, L., MacAry, P. A. & Ng, L. F. P. The trinity of COVID-19: immunity, inflammation and intervention. Nat. Rev. Immunol. 20, 363–374 (2020).
71. Thoms, M. et al. Structural basis for translational shutdown and immune evasion by the Nsp1 protein of SARS-CoV-2. Science 369, 1249–1255 (2020).
72. Wang, J. *et al.* COVID-19 confirmed patients with negative antibodies results. *BMC Infect. Dis.* **20**, 1–4 (2020).
73. Wang, N. et al. Retrospective Multicenter Cohort Study Shows Early Interferon Therapy Is Associated with Favorable Clinical Responses in COVID-19 Patients. Cell Host Microbe 28, 1–10 (2020).
74. Wang, Y. et al. GSA: Genome Sequence Archive*. Genomics, Proteomics Bioinformatics. 15, 14–18 (2017).
75. Weiner 3rd, J. & Domaszewska, T. tmod: an R package for general and multivariate enrichment analysis. PeerJ 4, 1–9 (2016).
76. Williamson, E. J. et al. OpenSAFELY: factors associated with COVID-19 death in 17 million patients. Nature (2020) doi:10.1038/s41586-020-2521-4.
77. Wrapp, D. et al. Cryo-EM structure of the 2019-nCoV spike in the prefusion conformation. Science 367, 1260–1263 (2020).
78. Wu, D. et al. ROAST: Rotation gene set tests for complex microarray experiments. Bioinformatics 26, 2176–2182 (2010).
79. Wu, K. E., Fazal, F. M., Parker, K. R., Zou, J. & Chang, H. Y. RNA-GPS Predicts SARS-CoV-2 RNA Residency to Host Mitochondria and Nucleolus. Cell Syst. 11, 102-108 (2020).
80. Wyler, E. et al. Bulk and single-cell gene expression profiling of SARS-CoV-2 infected human cell lines identifies molecular targets for therapeutic intervention. bioRxiv (2020).
81. Xiong, Y. et al. Transcriptomic characteristics of bronchoalveolar lavage fluid and peripheral blood mononuclear cells in COVID-19 patients. Emerg. Microbes Infect. 9, 761–770 (2020).
82. Yoshizumi, T. et al. RLR-mediated antiviral innate immunity requires oxidative phosphorylation activity. Sci. Rep. 7, 1–12 (2017).
83. Zeidler, R. et al. Downregulation of TAP1 in B lymphocytes by cellular and Epstein-Barr virus-

encoded interleukin-10. Blood 90, 2390–2397 (1997).

84. Zhang, Q. et al. Inborn errors of type I IFN immunity in patients with life-threatening COVID-19. Science 370, eabd4570 (2020).
85. Zhang, Z. et al. Database Resources of the National Genomics Data Center in 2020. Nucleic Acids Res. 48, D24–D33 (2020).
86. Zhao M. Cytokine storm and immunomodulatory therapy in COVID-19: role of chloroquine and anti-IL-6 monoclonal antibodies.Int J Antimicrob Agents. 55 (2020).
87. Zhao Y, Zixian Zhao, Yujia Wang, Yueqing Zhou, Yu Ma, W. Z. Single-cell RNA expression profiling of ACE2, the receptor of SARS-CoV-2. bioRxiv (2020).
88. Zhou, P. et al. A pneumonia outbreak associated with a new coronavirus of probable bat origin. Nature 579, 270–273 (2020).
89. Zhu, J., Duan, G., Wang, H., Cao, M. & Liu, Y. TREM-1 activation modulates dsRNA induced antiviral immunity with specific enhancement of MAPK signaling and the RLRs and TLRs on macrophages. Exp. Cell Res. 345, 70–81 (2016).

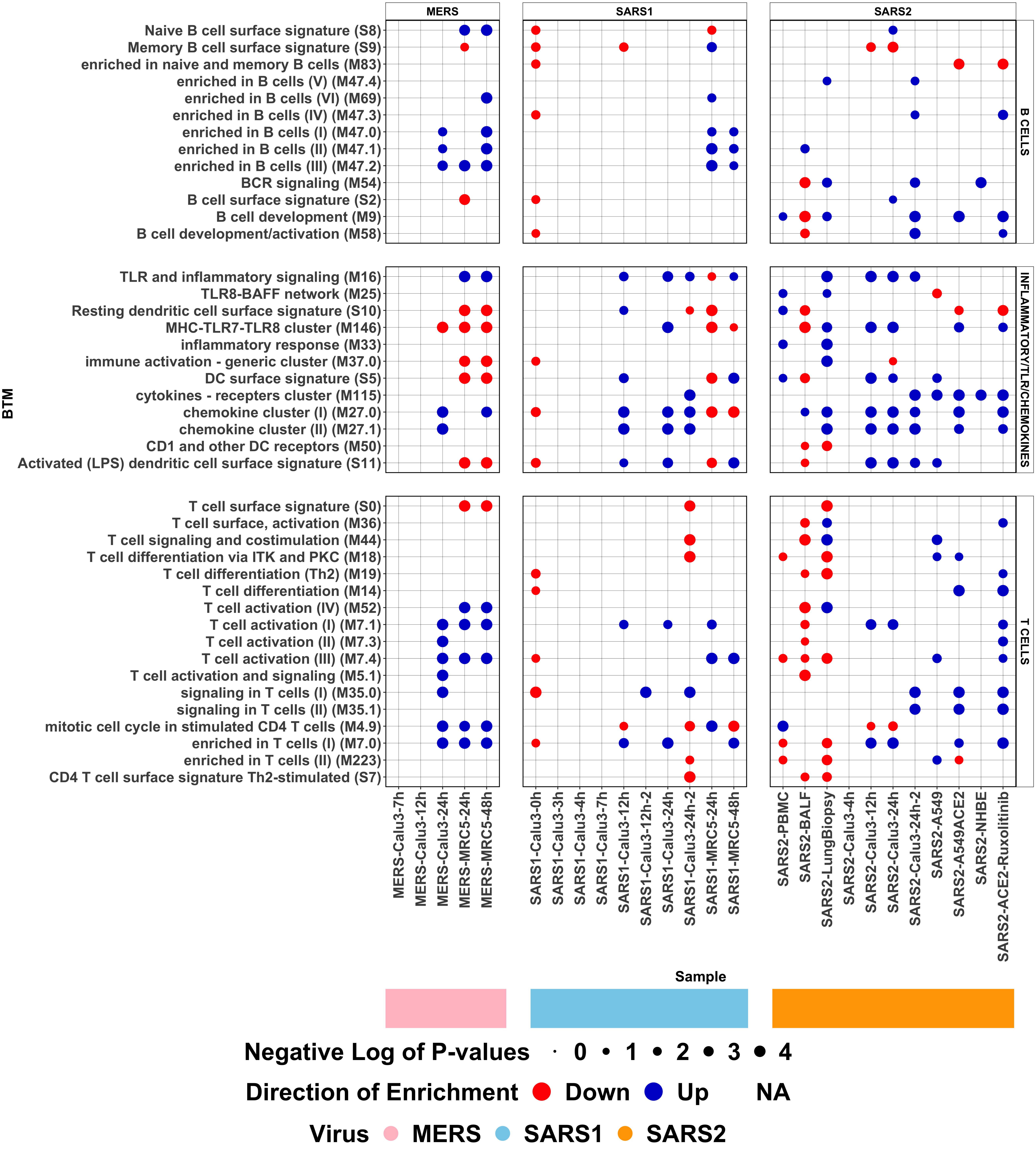
MERS
SARS1
SARS2
B CELLS
INFLAMMATORY/TLR/CHEMOKINES
T CELLS
BTM
Naive B cell surface signature (S8)
Memory B cell surface signature (S9)
enriched in naive and memory B cells (M83)
enriched in B cells (V) (M47.4)
enriched in B cells (VI) (M69)
enriched in B cells (IV) (M47.3)
enriched in B cells (I) (M47.0)
enriched in B cells (II) (M47.1)
enriched in B cells (III) (M47.2)
BCR signaling (M54)
B cell surface signature (S2)
B cell development (M9)
B cell development/activation (M58)
TLR and inflammatory signaling (M16)
TLR8-BAFF network (M25)
Resting dendritic cell surface signature (S10)
MHC-TLR7-TLR8 cluster (M146)
inflammatory response (M33)
immune activation - generic cluster (M37.0)
DC surface signature (S5)
cytokines - recepters cluster (M115)
chemokine cluster (I) (M27.0)
chemokine cluster (II) (M27.1)
CD1 and other DC receptors (M50)
Activated (LPS) dendritic cell surface signature (S11)
T cell surface signature (S0)
T cell surface, activation (M36)
T cell signaling and costimulation (M44)
T cell differentiation via ITK and PKC (M18)
T cell differentiation (Th2) (M19)
T cell differentiation (M14)
T cell activation (IV) (M52)
T cell activation (I) (M7.1)
T cell activation (II) (M7.3)
T cell activation (III) (M7.4)
T cell activation and signaling (M5.1)
signaling in T cells (I) (M35.0)
signaling in T cells (II) (M35.1)
mitotic cell cycle in stimulated CD4 T cells (M4.9)
enriched in T cells (I) (M7.0)
enriched in T cells (II) (M223)
CD4 T cell surface signature Th2-stimulated (S7)
MERS-Calu3-7h
MERS-Calu3-12h
MERS-Calu3-24h
MERS-MRC5-24h
MERS-MRC5-48h
SARS1-Calu3-0h
SARS1-Calu3-3h
SARS1-Calu3-4h
SARS1-Calu3-7h
SARS1-Calu3-12h
SARS1-Calu3-12h-2
SARS1-Calu3-24h
SARS1-Calu3-24h-2
SARS1-MRC5-24h
SARS1-MRC5-48h
SARS2-PBMC
SARS2-BALF
SARS2-LungBiopsy
SARS2-Calu3-4h
SARS2-Calu3-12h
SARS2-Calu3-24h
SARS2-Calu3-24h-2
SARS2-A549
SARS2-A549ACE2
SARS2-NHBE
SARS2-ACE2-Ruxolitinib
Sample
Negative Log of P-values 0 1 2 3 4
Direction of Enrichment ● Down ● Up NA
Virus ● MERS ● SARS1 ● SARS2

BALF_Covid19
Lungbiopsy_Covid19
PBMC_Covid19
antigen presentation (lipids and proteins) (M28)
enriched in antigen presentation (III) (M95.1)
enriched in antigen presentation (II) (M95.0)
enriched in antigen presentation (I) (M71)
regulation of antigen presentation and immune response (M5.0)
ANTIGEN PRESENTATION
B cell development/activation (M58)
B cell development (M9)
BCR signaling (M54)
enriched in B cells (II) (M47.1)
enriched in B cells (IV) (M47.3)
enriched in B cells (VI) (M69)
B CELLS
cell cycle and growth arrest (M31)
cell cycle and transcription (M4.0)
cell cycle (III) (M103)
cell cycle (II) (M4.10)
cell cycle (I) (M4.1)
cell cycle, mitotic phase (M230)
cell division - E2F transcription network (M4.8)
cell division in stimulated CD4 T cells (M4.6)
cell division (M37.3)
cell division (stimulated CD4+ T cells) (M46)
DNA repair (M76)
E2F transcription factor network (M8)
enriched in cell cycle (M167)
mismatch repair (II) (M22.1)
mismatch repair (I) (M22.0)
mitosis (TF motif CCAATNNSNNNGCG) (M169)
mitotic cell cycle - DNA replication (M4.4)
mitotic cell cycle in stimulated CD4 T cells (M4.11)
mitotic cell cycle in stimulated CD4 T cells (M4.5)
mitotic cell cycle (M4.7)
mitotic cell division (M6)
Ran mediated mitosis (M15)
CELL CYCLE
activated dendritic cells (M67)
chemokines and inflammatory molecules in myeloid cells (M86.0)
complement and other receptors in DCs (M40)
enriched in activated dendritic cells (II) (M165)
enriched in activated dendritic cells (I) (M119)
enriched in activated dendritic cells/monocytes (M64)
enriched in dendritic cells (M168)
inflammasome receptors and signaling (M53)
myeloid, dendritic cell activation via NFkB (II) (M43.1)
myeloid, dendritic cell activation via NFkB (I) (M43.0)
proinflammatory dendritic cell, myeloid cell response (M86.1)
DC ACTIVATION
adhesion and migration, chemotaxis (M91)
amino acid metabolism and transport (M154.0)
cell adhesion (GO) (M117)
cell adhesion, membrane (M133.0)
cell movement, Adhesion & Platelet activation (M30)
cytoskeletal remodeling (M32.8)
cytoskeleton/actin (SRF transcription targets) (M145.1)
enriched for cell migration (M122)
extracellular matrix, complement (M140)
extracellular matrix (I) (M2.0)
integrin cell surface interactions (II) (M1.1)
integrin mediated leukocyte migration (M39)
leukocyte migration (M88.0)
receptors, cell migration (M109)
regulation of localization (GO) (M63)
respiratory electron transport chain (mitochondrion) (M216)
respiratory electron transport chain (mitochondrion) (M219)
respiratory electron transport chain (mitochondrion) (M231)
respiratory electron transport chain (mitochondrion) (M238)
ECM AND MIGRATION
Activated (LPS) dendritic cell surface signature (S11)
CD1 and other DC receptors (M50)
chemokine cluster (II) (M27.1)
chemokine cluster (I) (M27.0)
DC surface signature (S5)
immune activation - generic cluster (M37.0)
inflammatory response (M33)
MHC-TLR7-TLR8 cluster (M146)
Resting dendritic cell surface signature (S10)
TLR8-BAFF network (M25)
TLR and inflammatory signaling (M16)
INFLAMMATORY/TLR/CHEMOKINES
antiviral IFN signature (M75)
innate activation by cytosolic DNA sensing (M13)
innate antiviral response (M150)
type I interferon response (M127)
viral sensing & immunity; IRF2 targets network (II) (M111.1)
viral sensing & immunity; IRF2 targets network (I) (M111.0)
INTERFERON/ANTIVIRAL SENSING
enriched in monocytes (II) (M11.0)
enriched in monocytes (I) (M4.15)
enriched in monocytes (IV) (M118.0)
enriched in monocytes (surface) (M118.1)
enriched in myeloid cells and monocytes (M81)
Monocyte surface signature (S4)
RA, WNT, CSF receptors network (monocyte) (M23)
MONOCYTES
enriched in neutrophils (I) (M37.1)
formyl peptide receptor mediated neutrophil response (M11.2)
NEUTROPHILS
enriched in NK cells (III) (M157)
enriched in NK cells (II) (M61.0)
enriched in NK cells (I) (M7.2)
enriched in NK cells (receptor activation) (M61.2)
NK cell surface signature (S1)
NK CELLS
AP-1 transcription factor network (M20)
blood coagulation (M11.1)
cell activation (IL15, IL23, TNF) (M24)
cell cycle, ATP binding (M144)
cell junction (GO) (M4.13)
cell junction (M162.1)
chaperonin mediated protein folding (II) (M204.1)
chaperonin mediated protein folding (I) (M204.0)
chemokines and receptors (M38)
C-MYC transcriptional network (M4.12)
collagen, TGFB family et al (M77)
complement activation (I) (M112.0)
CORO1A-DEF6 network (II) (M32.4)
CORO1A-DEF6 network (I) (M32.2)
double positive thymocytes (M126)
E2F1 targets (Q3) (M10.0)
E2F1 targets (Q4) (M10.1)
endoplasmic reticulum (M37.2)
enriched for TF motif TNCATNTCCYR (M232)
enriched for ubiquitination (M138)
enriched for unknown TF motif CTCNANGTGNY (M62.1)
enriched in DNA interacting proteins (M182)
erythrocyte differentiation (M173)
extracellular matrix, collagen (M210)
extracellular matrix (II) (M2.1)
extracellular region cluster (GO) (M189)
golgi membrane (II) (M237)
growth factor induced, enriched in nuclear receptor subfamily 4 (M94)
heme biosynthesis (II) (M222)
Hox cluster III (M17.2)
immuregulation - monocytes, T and B cells (M57)
intracellular transport (M147)
KLF12 targets network (M32.3)
leukocyte activation and migration (M45)
leukocyte differentiation (M160)
lymphocyte generic cluster (M60)
lysosomal/endosomal proteins (M139)
Membrane, ER proteins (M134)
mitochondrial cluster (M235)
myeloid cell enriched receptors and transporters (M4.3)
nuclear pore complex (M106.0)
nuclear pore complex (mitosis) (M106.1)
nuclear pore, transport; mRNA splicing, processing (M143)
plasma membrane, cell junction (M162.0)
platelet activation - actin binding (M196)
platelet activation and degranulation (M85)
platelet activation (III) (M42)
platelet activation (II) (M32.1)
platelet activation (I) (M32.0)
proteasome (M226)
purine nucleotide biosynthesis (M212)
regulation of transcription, transcription factors (M213)
spliceosome (M250)
T & B cell development, activation (M62.0)
transcriptional targets of glucocorticoid receptor (M74)
transcription elongation, RNA polymerase II (M234)
transcription regulation in cell development (M49)
translation initiation (M227)
transmembrane transport (II) (M191)
transmembrane transport (I) (M87)
OTHERS
enriched in B cell differentiation (M123)
plasma cells, immunoglobulins (M156.1)
Plasma cell surface signature (S3)
PLASMA CELLS
CCR1, 7 and cell signaling (M59)
G protein mediated calcium signaling (M159)
IL2, IL7, TCR network (M65)
inositol phosphate metabolism (M129)
MAPK, RAS signaling (M100)
phosphatidylinositol signaling system (M101)
PLK1 signaling events (M4.2)
putative targets of PAX3 (M89.0)
putative targets of PAX3 (M89.1)
small GTPase mediated signal transduction (M215)
suppression of MAPK signaling (M56)
Wnt signaling pathway (M206)
SIGNAL TRANSDUCTION
CD4 T cell surface signature Th2-stimulated (S7)
enriched in T cells (II) (M223)
enriched in T cells (I) (M7.0)
mitotic cell cycle in stimulated CD4 T cells (M4.9)
signaling in T cells (I) (M35.0)
T cell activation and signaling (M5.1)
T cell activation (III) (M7.4)
T cell activation (II) (M7.3)
T cell activation (I) (M7.1)
T cell activation (IV) (M52)
T cell differentiation (M14)
T cell differentiation (Th2) (M19)
T cell differentiation via ITK and PKC (M18)
T cell signaling and costimulation (M44)
T cell surface, activation (M36)
T cell surface signature (S0)
T CELLS
Negative log of P-values
0 1 2 3 4

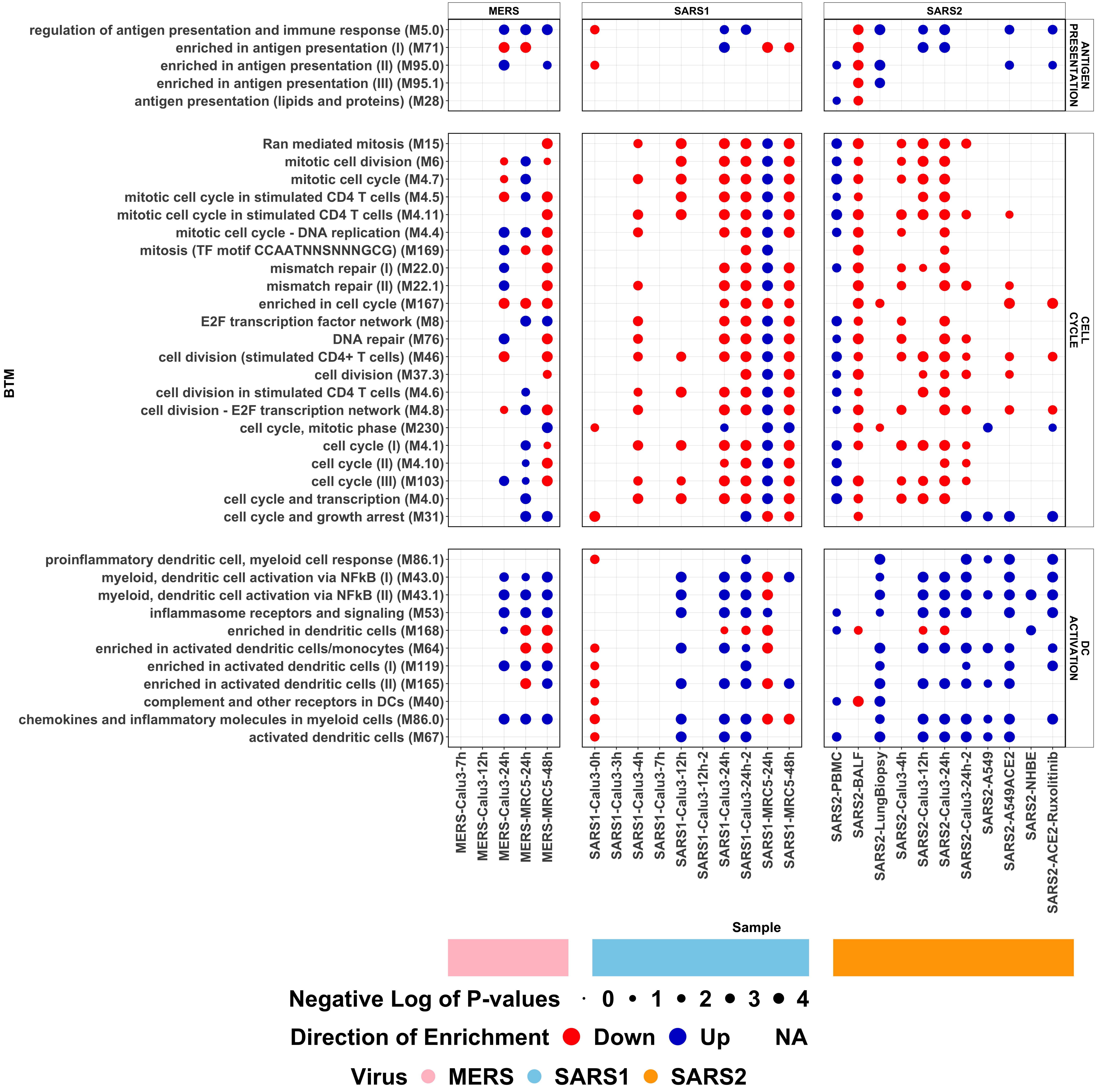
MERS
SARS1
SARS2
ANTIGEN PRESENTATION
CELL CYCLE
DC ACTIVATION
BTM
regulation of antigen presentation and immune response (M5.0)
enriched in antigen presentation (I) (M71)
enriched in antigen presentation (II) (M95.0)
enriched in antigen presentation (III) (M95.1)
antigen presentation (lipids and proteins) (M28)
Ran mediated mitosis (M15)
mitotic cell division (M6)
mitotic cell cycle (M4.7)
mitotic cell cycle in stimulated CD4 T cells (M4.5)
mitotic cell cycle in stimulated CD4 T cells (M4.11)
mitotic cell cycle - DNA replication (M4.4)
mitosis (TF motif CCAATNNSNNNGCG) (M169)
mismatch repair (I) (M22.0)
mismatch repair (II) (M22.1)
enriched in cell cycle (M167)
E2F transcription factor network (M8)
DNA repair (M76)
cell division (stimulated CD4+ T cells) (M46)
cell division (M37.3)
cell division in stimulated CD4 T cells (M4.6)
cell division - E2F transcription network (M4.8)
cell cycle, mitotic phase (M230)
cell cycle (I) (M4.1)
cell cycle (II) (M4.10)
cell cycle (III) (M103)
cell cycle and transcription (M4.0)
cell cycle and growth arrest (M31)
proinflammatory dendritic cell, myeloid cell response (M86.1)
myeloid, dendritic cell activation via NFkB (I) (M43.0)
myeloid, dendritic cell activation via NFkB (II) (M43.1)
inflammasome receptors and signaling (M53)
enriched in dendritic cells (M168)
enriched in activated dendritic cells/monocytes (M64)
enriched in activated dendritic cells (I) (M119)
enriched in activated dendritic cells (II) (M165)
complement and other receptors in DCs (M40)
chemokines and inflammatory molecules in myeloid cells (M86.0)
activated dendritic cells (M67)
MERS-Calu3-7h
MERS-Calu3-12h
MERS-Calu3-24h
MERS-MRC5-24h
MERS-MRC5-48h
SARS1-Calu3-0h
SARS1-Calu3-3h
SARS1-Calu3-4h
SARS1-Calu3-7h
SARS1-Calu3-12h
SARS1-Calu3-12h-2
SARS1-Calu3-24h
SARS1-Calu3-24h-2
SARS1-MRC5-24h
SARS1-MRC5-48h
SARS2-PBMC
SARS2-BALF
SARS2-LungBiopsy
SARS2-Calu3-4h
SARS2-Calu3-12h
SARS2-Calu3-24h
SARS2-Calu3-24h-2
SARS2-A549
SARS2-A549ACE2
SARS2-NHBE
SARS2-ACE2-Ruxolitinib
Sample
Negative Log of P-values 0 1 2 3 4
Direction of Enrichment Down Up NA
Virus MERS SARS1 SARS2

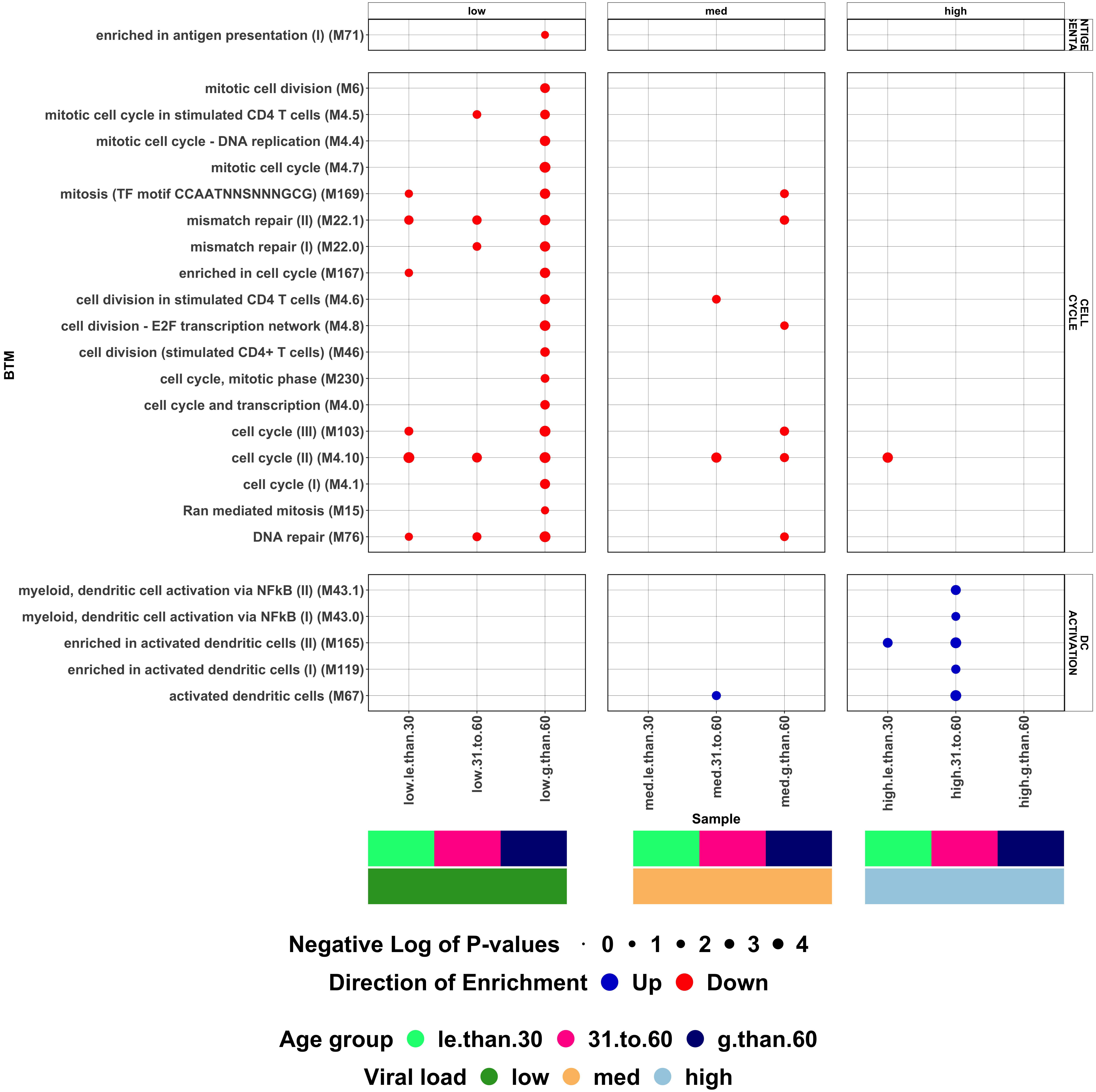
low
med
high
enriched in antigen presentation (I) (M71)
mitotic cell division (M6)
mitotic cell cycle in stimulated CD4 T cells (M4.5)
mitotic cell cycle - DNA replication (M4.4)
mitotic cell cycle (M4.7)
mitosis (TF motif CCAATNNSNNNGCG) (M169)
mismatch repair (II) (M22.1)
mismatch repair (I) (M22.0)
enriched in cell cycle (M167)
cell division in stimulated CD4 T cells (M4.6)
cell division - E2F transcription network (M4.8)
cell division (stimulated CD4+ T cells) (M46)
cell cycle, mitotic phase (M230)
cell cycle and transcription (M4.0)
cell cycle (III) (M103)
cell cycle (II) (M4.10)
cell cycle (I) (M4.1)
Ran mediated mitosis (M15)
DNA repair (M76)
myeloid, dendritic cell activation via NFkB (II) (M43.1)
myeloid, dendritic cell activation via NFkB (I) (M43.0)
enriched in activated dendritic cells (II) (M165)
enriched in activated dendritic cells (I) (M119)
activated dendritic cells (M67)
BTM
NTIGE SENTA
CELL CYCLE
DC ACTIVATION
low.le.than.30
low.31.to.60
low.g.than.60
med.le.than.30
med.31.to.60
med.g.than.60
high.le.than.30
high.31.to.60
high.g.than.60
Sample
Negative Log of P-values 0 1 2 3 4
Direction of Enrichment Up Down
Age group le.than.30 31.to.60 g.than.60
Viral load low med high

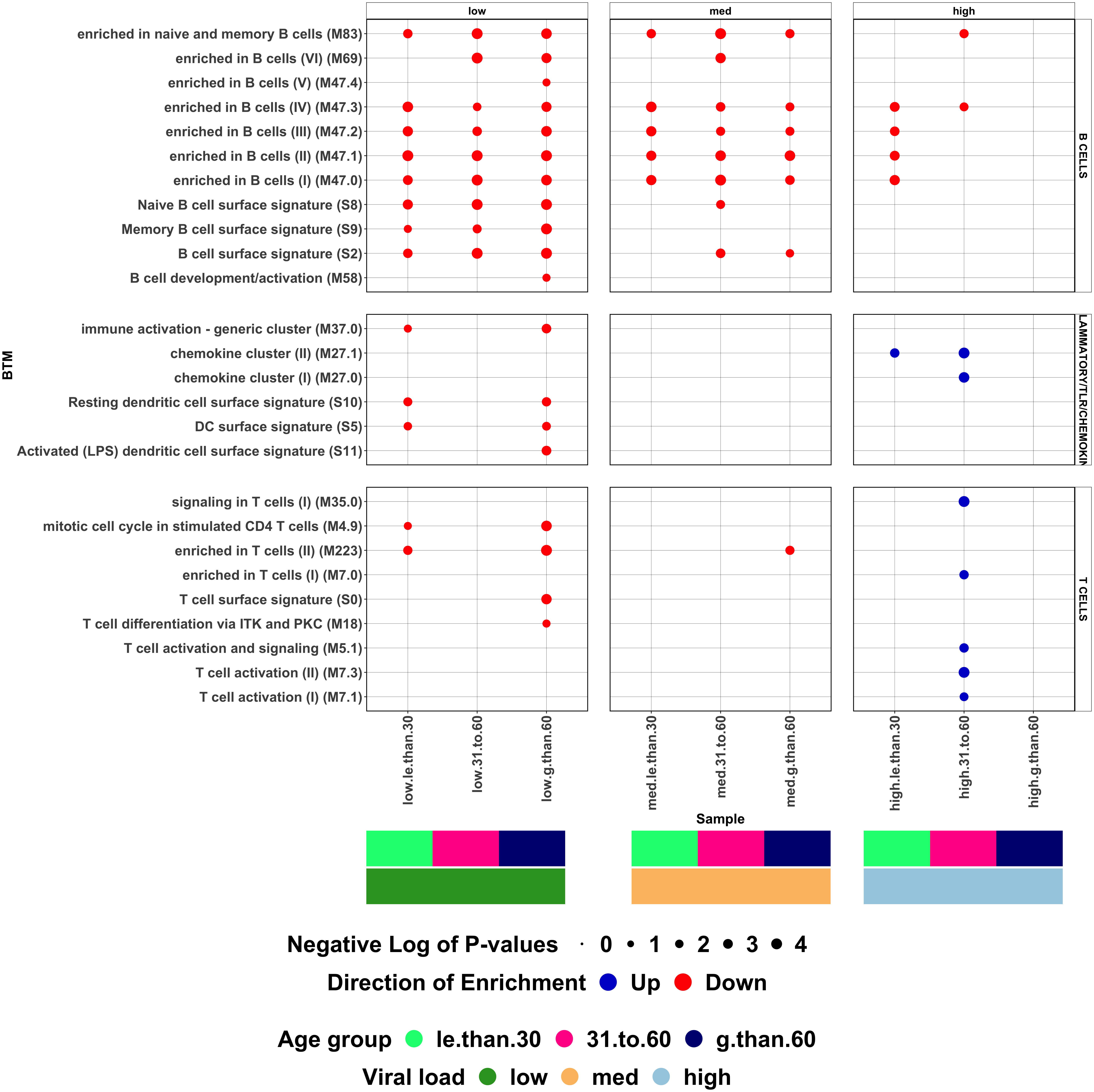
low
med
high
enriched in naive and memory B cells (M83)
enriched in B cells (VI) (M69)
enriched in B cells (V) (M47.4)
enriched in B cells (IV) (M47.3)
enriched in B cells (III) (M47.2)
enriched in B cells (II) (M47.1)
enriched in B cells (I) (M47.0)
Naive B cell surface signature (S8)
Memory B cell surface signature (S9)
B cell surface signature (S2)
B cell development/activation (M58)
B CELLS
immune activation - generic cluster (M37.0)
chemokine cluster (II) (M27.1)
chemokine cluster (I) (M27.0)
Resting dendritic cell surface signature (S10)
DC surface signature (S5)
Activated (LPS) dendritic cell surface signature (S11)
LAMMATORY/TLR/CHEMOKIN
signaling in T cells (I) (M35.0)
mitotic cell cycle in stimulated CD4 T cells (M4.9)
enriched in T cells (II) (M223)
enriched in T cells (I) (M7.0)
T cell surface signature (S0)
T cell differentiation via ITK and PKC (M18)
T cell activation and signaling (M5.1)
T cell activation (II) (M7.3)
T cell activation (I) (M7.1)
T CELLS
BTM
low.le.than.30
low.31.to.60
low.g.than.60
med.le.than.30
med.31.to.60
med.g.than.60
high.le.than.30
high.31.to.60
high.g.than.60
Sample
Negative Log of P-values 0 1 2 3 4
Direction of Enrichment Up Down
Age group le.than.30 31.to.60 g.than.60
Viral load low med high

MERS-MRC5-48h
SARS1-MRC5-24h
MERS-MRC5-24h
SARS1-Calu3-24h-2
SARS2-ACE2-Ruxolitinib
SARS2-A549ACE2
SARS2-BALF
SARS1-MRC5-48h
MERS-Calu3-24h
SARS2-LungBiopsy
SARS2-Calu3-24h
SARS1-Calu3-24h
SARS2-Calu3-12h
SARS1-Calu3-12h
SARS2-PBMC
SARS2-Calu3-24h-2
SARS1-Calu3-0h
SARS2-A549
SARS2-Calu3-4h
SARS1-Calu3-4h
SARS2-NHBE
SARS1-Calu3-3h
SARS1-Calu3-12h-2
MERS-Calu3-12h
SARS1-Calu3-7h
MERS-Calu3-7h
ANTIGEN PRESENTATION
B CELLS
CELL CYCLE
DC ACTIVATION
ECM AND MIGRATION
INFLAMMATORY/TLR/CHEMOKINES
INTERFERON/ANTIVIRAL SENSING
MONOCYTES
NEUTROPHILS
NK CELLS
OTHERS
PLASMA CELLS
SIGNAL TRANSDUCTION
T CELLS
Negative log of P-values
0 1 2 3 4

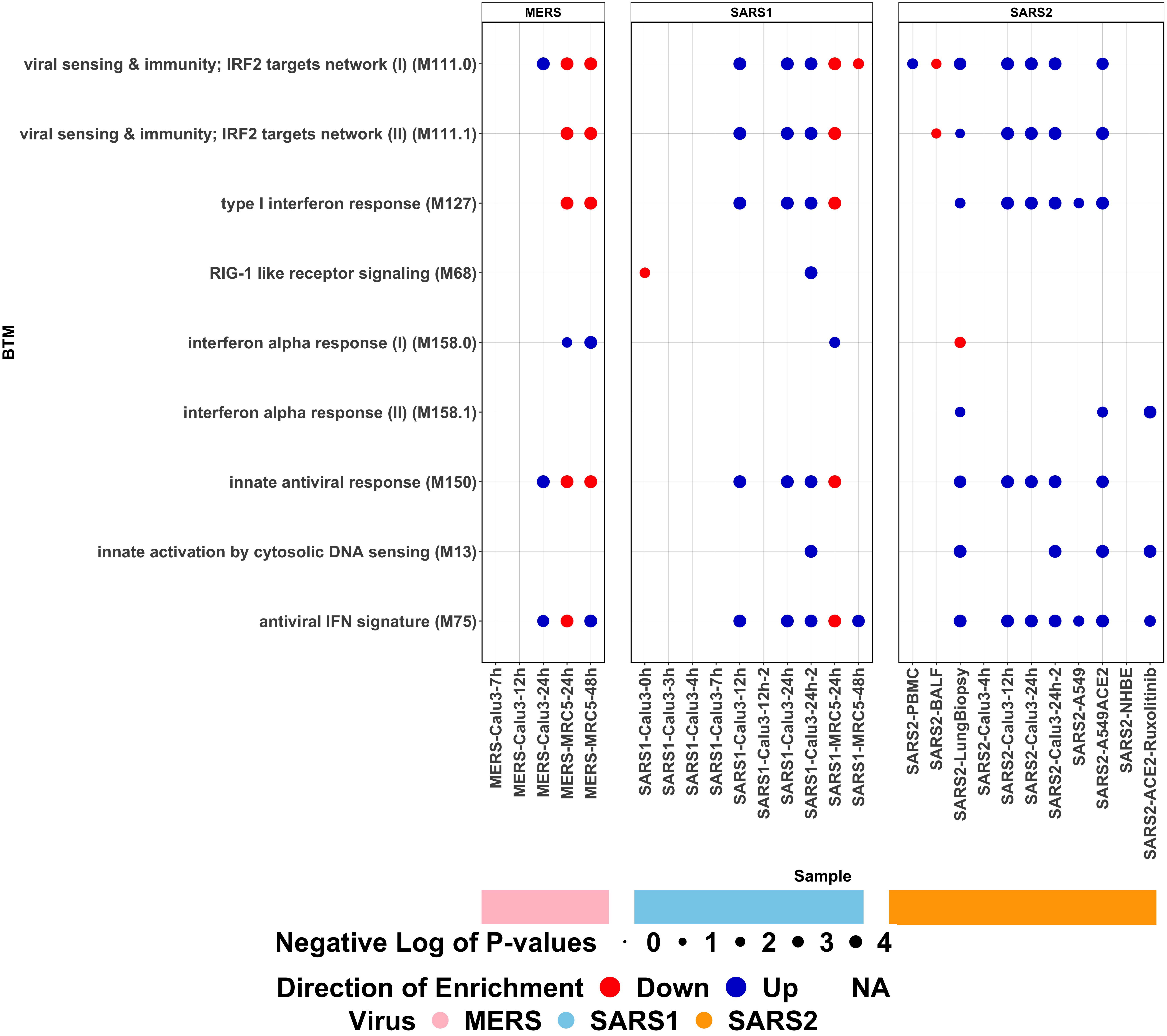
MERS
SARS1
SARS2
BTM
viral sensing & immunity; IRF2 targets network (I) (M111.0)
viral sensing & immunity; IRF2 targets network (II) (M111.1)
type I interferon response (M127)
RIG-1 like receptor signaling (M68)
interferon alpha response (I) (M158.0)
interferon alpha response (II) (M158.1)
innate antiviral response (M150)
innate activation by cytosolic DNA sensing (M13)
antiviral IFN signature (M75)
MERS-Calu3-7h
MERS-Calu3-12h
MERS-Calu3-24h
MERS-MRC5-24h
MERS-MRC5-48h
SARS1-Calu3-0h
SARS1-Calu3-3h
SARS1-Calu3-4h
SARS1-Calu3-7h
SARS1-Calu3-12h
SARS1-Calu3-12h-2
SARS1-Calu3-24h
SARS1-Calu3-24h-2
SARS1-MRC5-24h
SARS1-MRC5-48h
SARS2-PBMC
SARS2-BALF
SARS2-LungBiopsy
SARS2-Calu3-4h
SARS2-Calu3-12h
SARS2-Calu3-24h
SARS2-Calu3-24h-2
SARS2-A549
SARS2-A549ACE2
SARS2-NHBE
SARS2-ACE2-Ruxolitinib
Sample
Negative Log of P-values 0 1 2 3 4
Direction of Enrichment Down Up NA
Virus MERS SARS1 SARS2

low
med
high
viral sensing & immunity; IRF2 targets network (II) (M111.1)
viral sensing & immunity; IRF2 targets network (I) (M111.0)
type I interferon response (M127)
innate antiviral response (M150)
innate activation by cytosolic DNA sensing (M13)
antiviral IFN signature (M75)
BTM
low.le.than.30
low.31.to.60
low.g.than.60
med.le.than.30
med.31.to.60
med.g.than.60
high.le.than.30
high.31.to.60
high.g.than.60
Sample
Negative Log of P-values 0 1 2 3 4
Direction of Enrichment Up
Age group le.than.30 31.to.60 g.than.60
Viral load low med high

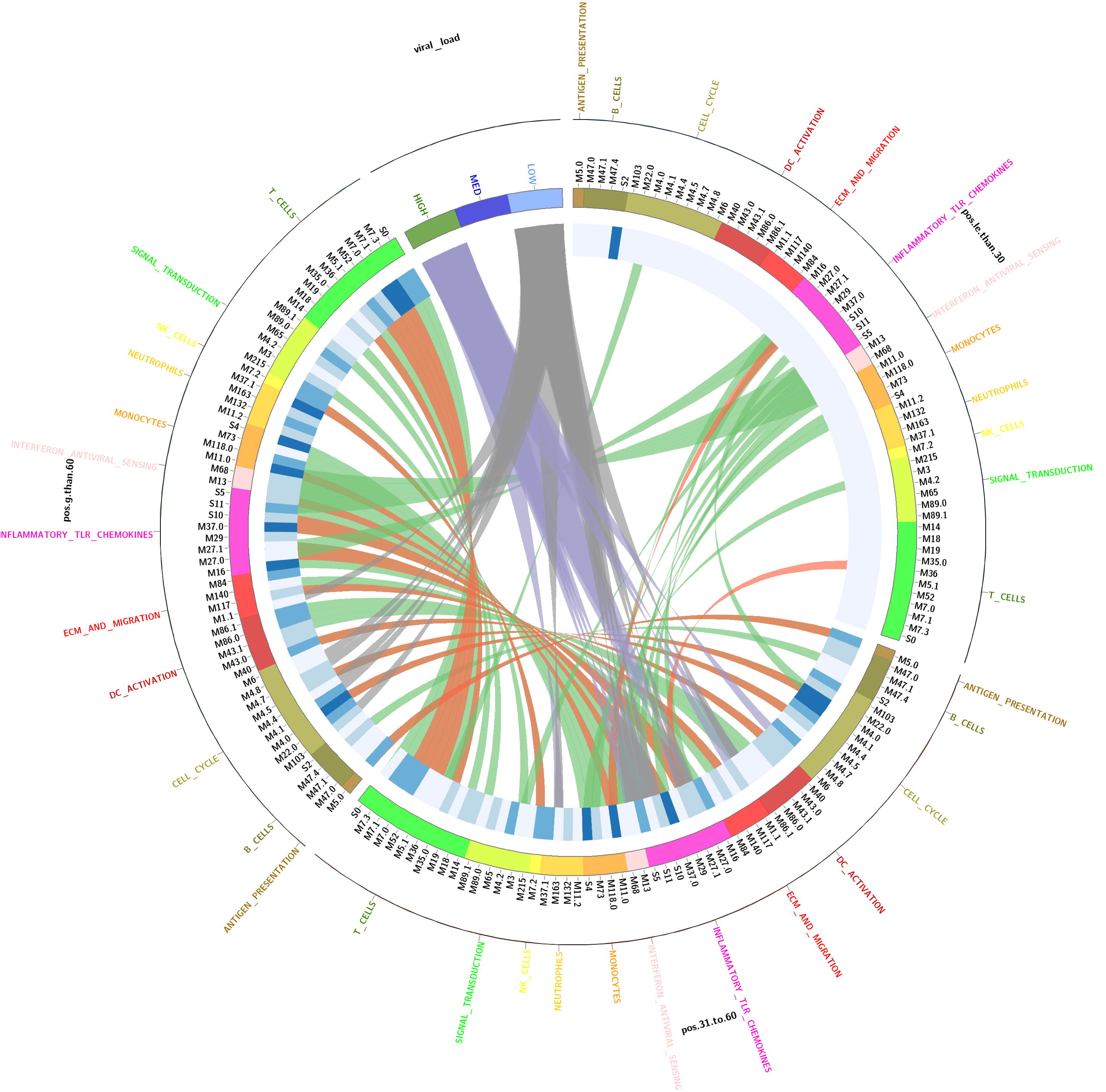
viral _load
HIGH
MED
LOW
pos.le.than.30
pos.g.than.60
pos.31.to.60
ANTIGEN_PRESENTATION
B_CELLS
CELL_CYCLE
DC_ACTIVATION
ECM_AND_MIGRATION
INFLAMMATORY_TLR_CHEMOKINES
INTERFERON_ANTIVIRAL_SENSING
MONOCYTES
NEUTROPHILS
NK_CELLS
SIGNAL_TRANSDUCTION
T_CELLS
M5.0
M47.0
M47.1
M47.4
S2
M103
M22.0
M4.0
M4.1
M4.4
M4.5
M4.7
M4.8
M6
M40
M43.0
M43.1
M86.0
M86.1
M1.1
M117
M140
M84
M16
M27.0
M27.1
M29
M37.0
S10
S11
S5
M13
M68
M11.0
M118.0
M73
S4
M11.2
M132
M163
M37.1
M7.2
M215
M3
M4.2
M65
M89.0
M89.1
M14
M18
M19
M35.0
M36
M5.1
M52
M7.0
M7.1
M7.3
S0

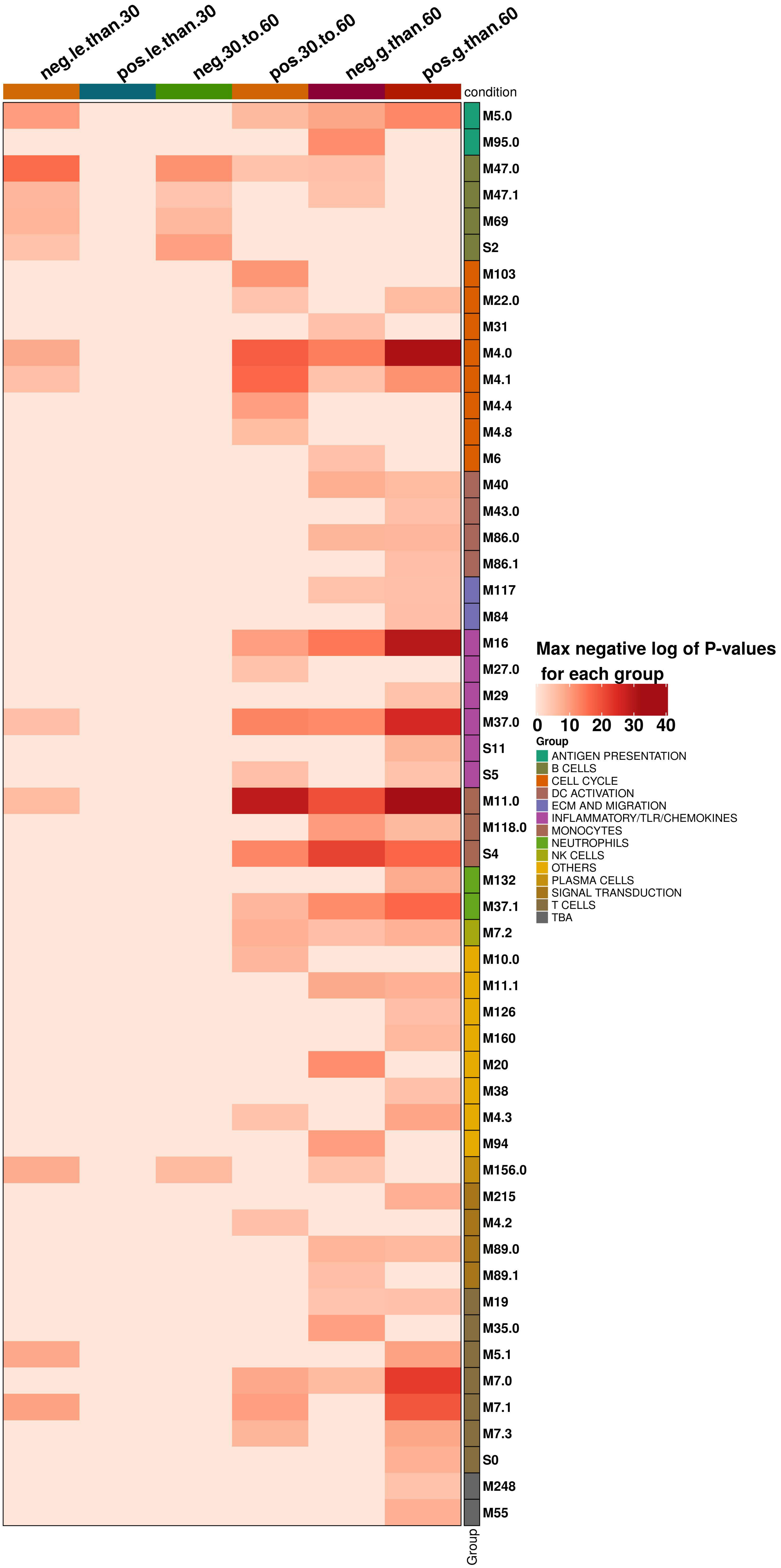
neg.le.than.30
pos.le.than.30
neg.30.to.60
pos.30.to.60
neg.g.than.60
pos.g.than.60
condition
M5.0
M95.0
M47.0
M47.1
M69
S2
M103
M22.0
M31
M4.0
M4.1
M4.4
M4.8
M6
M40
M43.0
M86.0
M86.1
M117
M84
M16
M27.0
M29
M37.0
S11
S5
M11.0
M118.0
S4
M132
M37.1
M7.2
M10.0
M11.1
M126
M160
M20
M38
M4.3
M94
M156.0
M215
M4.2
M89.0
M89.1
M19
M35.0
M5.1
M7.0
M7.1
M7.3
S0
M248
M55
Group
Max negative log of P-values
for each group
0
10
20
30
40
Group
ANTIGEN PRESENTATION
B CELLS
CELL CYCLE
DC ACTIVATION
ECM AND MIGRATION
INFLAMMATORY/TLR/CHEMOKINES
MONOCYTES
NEUTROPHILS
NK CELLS
OTHERS
PLASMA CELLS
SIGNAL TRANSDUCTION
T CELLS
TBA

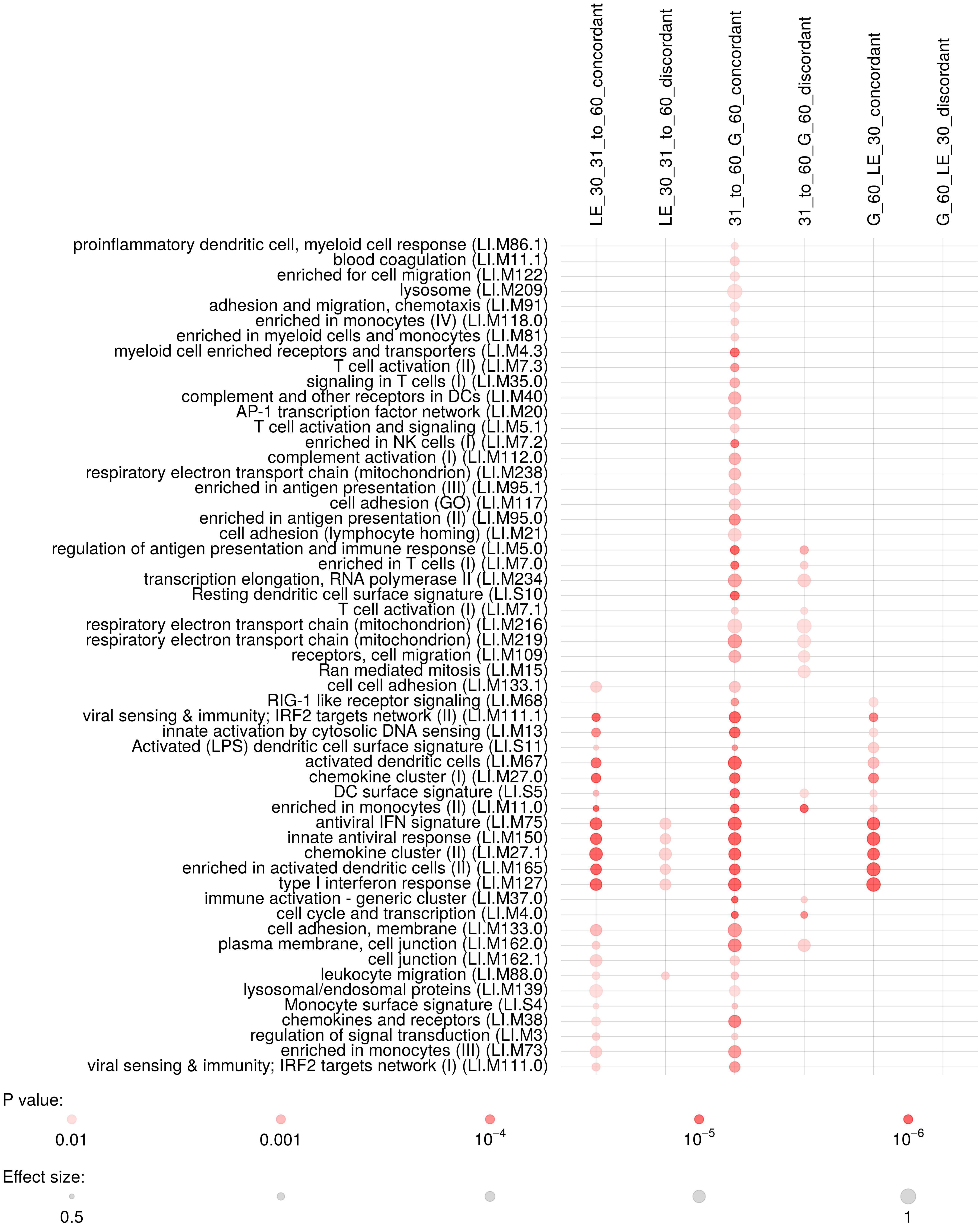
LE_30_31_to_60_concordant
LE_30_31_to_60_discordant
31_to_60_G_60_concordant
31_to_60_G_60_discordant
G_60_LE_30_concordant
G_60_LE_30_discordant
proinflammatory dendritic cell, myeloid cell response (LI.M86.1)
blood coagulation (LI.M11.1)
enriched for cell migration (LI.M122)
lysosome (LI.M209)
adhesion and migration, chemotaxis (LI.M91)
enriched in monocytes (IV) (LI.M118.0)
enriched in myeloid cells and monocytes (LI.M81)
myeloid cell enriched receptors and transporters (LI.M4.3)
T cell activation (II) (LI.M7.3)
signaling in T cells (I) (LI.M35.0)
complement and other receptors in DCs (LI.M40)
AP-1 transcription factor network (LI.M20)
T cell activation and signaling (LI.M5.1)
enriched in NK cells (I) (LI.M7.2)
complement activation (I) (LI.M112.0)
respiratory electron transport chain (mitochondrion) (LI.M238)
enriched in antigen presentation (III) (LI.M95.1)
cell adhesion (GO) (LI.M117)
enriched in antigen presentation (II) (LI.M95.0)
cell adhesion (lymphocyte homing) (LI.M21)
regulation of antigen presentation and immune response (LI.M5.0)
enriched in T cells (I) (LI.M7.0)
transcription elongation, RNA polymerase II (LI.M234)
Resting dendritic cell surface signature (LI.S10)
T cell activation (I) (LI.M7.1)
respiratory electron transport chain (mitochondrion) (LI.M216)
respiratory electron transport chain (mitochondrion) (LI.M219)
receptors, cell migration (LI.M109)
Ran mediated mitosis (LI.M15)
cell cell adhesion (LI.M133.1)
RIG-1 like receptor signaling (LI.M68)
viral sensing & immunity; IRF2 targets network (II) (LI.M111.1)
innate activation by cytosolic DNA sensing (LI.M13)
Activated (LPS) dendritic cell surface signature (LI.S11)
activated dendritic cells (LI.M67)
chemokine cluster (I) (LI.M27.0)
DC surface signature (LI.S5)
enriched in monocytes (II) (LI.M11.0)
antiviral IFN signature (LI.M75)
innate antiviral response (LI.M150)
chemokine cluster (II) (LI.M27.1)
enriched in activated dendritic cells (II) (LI.M165)
type I interferon response (LI.M127)
immune activation - generic cluster (LI.M37.0)
cell cycle and transcription (LI.M4.0)
cell adhesion, membrane (LI.M133.0)
plasma membrane, cell junction (LI.M162.0)
cell junction (LI.M162.1)
leukocyte migration (LI.M88.0)
lysosomal/endosomal proteins (LI.M139)
Monocyte surface signature (LI.S4)
chemokines and receptors (LI.M38)
regulation of signal transduction (LI.M3)
enriched in monocytes (III) (LI.M73)
viral sensing & immunity; IRF2 targets network (I) (LI.M111.0)
P value:
0.01
0.001
10^{-4}
10^{-5}
10^{-6}
Effect size:
0.5
1

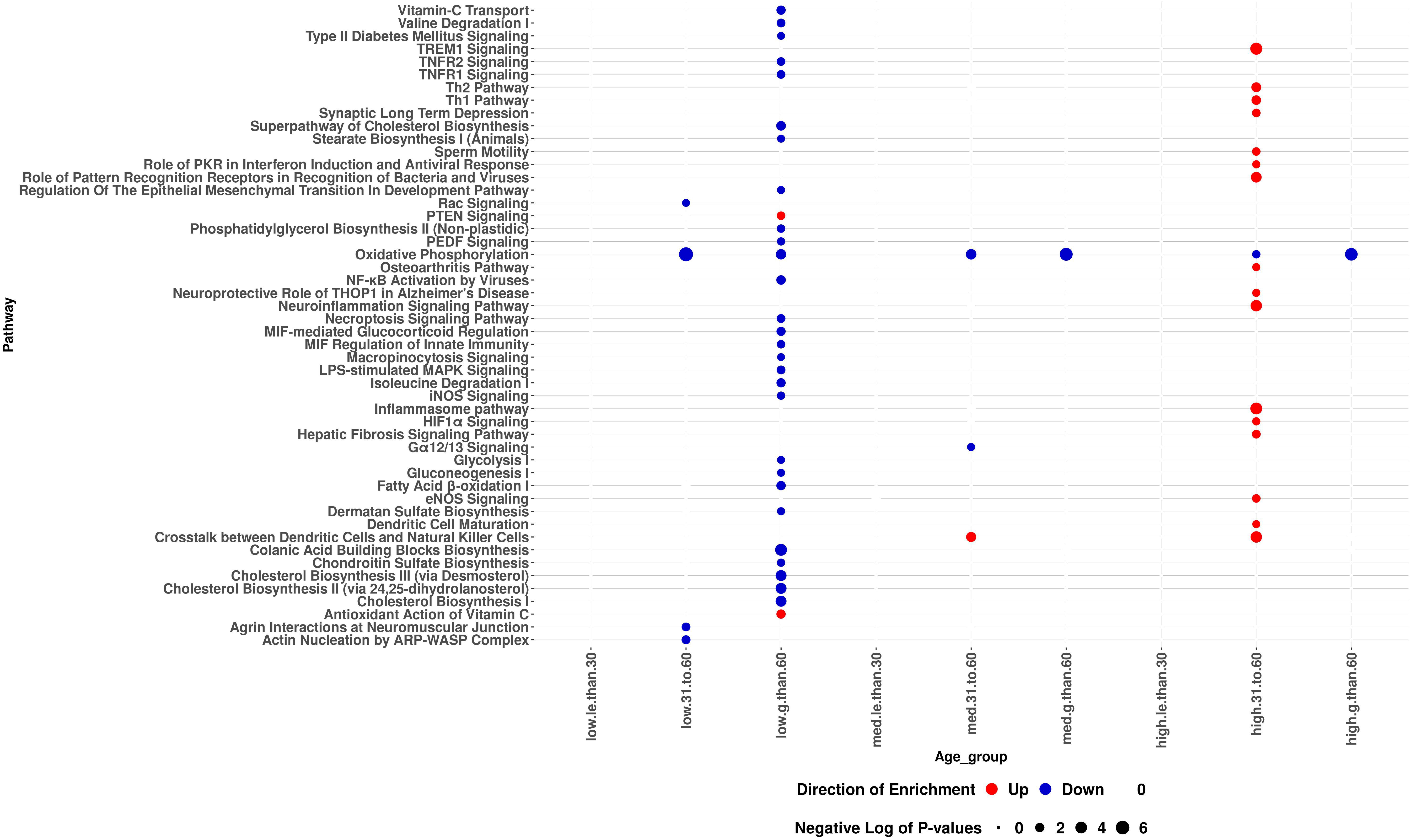
Vitamin-C Transport
Valine Degradation I
Type II Diabetes Mellitus Signaling
TREM1 Signaling
TNFR2 Signaling
TNFR1 Signaling
Th2 Pathway
Th1 Pathway
Synaptic Long Term Depression
Superpathway of Cholesterol Biosynthesis
Stearate Biosynthesis I (Animals)
Sperm Motility
Role of PKR in Interferon Induction and Antiviral Response
Role of Pattern Recognition Receptors in Recognition of Bacteria and Viruses
Regulation Of The Epithelial Mesenchymal Transition In Development Pathway
Rac Signaling
PTEN Signaling
Phosphatidylglycerol Biosynthesis II (Non-plastidic)
PEDF Signaling
Oxidative Phosphorylation
Osteoarthritis Pathway
NF-κB Activation by Viruses
Neuroprotective Role of THOP1 in Alzheimer's Disease
Neuroinflammation Signaling Pathway
Necroptosis Signaling Pathway
MIF-mediated Glucocorticoid Regulation
MIF Regulation of Innate Immunity
Macropinocytosis Signaling
LPS-stimulated MAPK Signaling
Isoleucine Degradation I
iNOS Signaling
Inflammasome pathway
HIF1α Signaling
Hepatic Fibrosis Signaling Pathway
Gα12/13 Signaling
Glycolysis I
Gluconeogenesis I
Fatty Acid β-oxidation I
eNOS Signaling
Dermatan Sulfate Biosynthesis
Dendritic Cell Maturation
Crosstalk between Dendritic Cells and Natural Killer Cells
Colanic Acid Building Blocks Biosynthesis
Chondroitin Sulfate Biosynthesis
Cholesterol Biosynthesis III (via Desmosterol)
Cholesterol Biosynthesis II (via 24,25-dihydrolanosterol)
Cholesterol Biosynthesis I
Antioxidant Action of Vitamin C
Agrin Interactions at Neuromuscular Junction
Actin Nucleation by ARP-WASP Complex
Pathway
low.le.than.30
low.31.to.60
low.g.than.60
med.le.than.30
med.31.to.60
med.g.than.60
high.le.than.30
high.31.to.60
high.g.than.60
Age_group
Direction of Enrichment
Up
Down
0
Negative Log of P-values
0
2
4
6

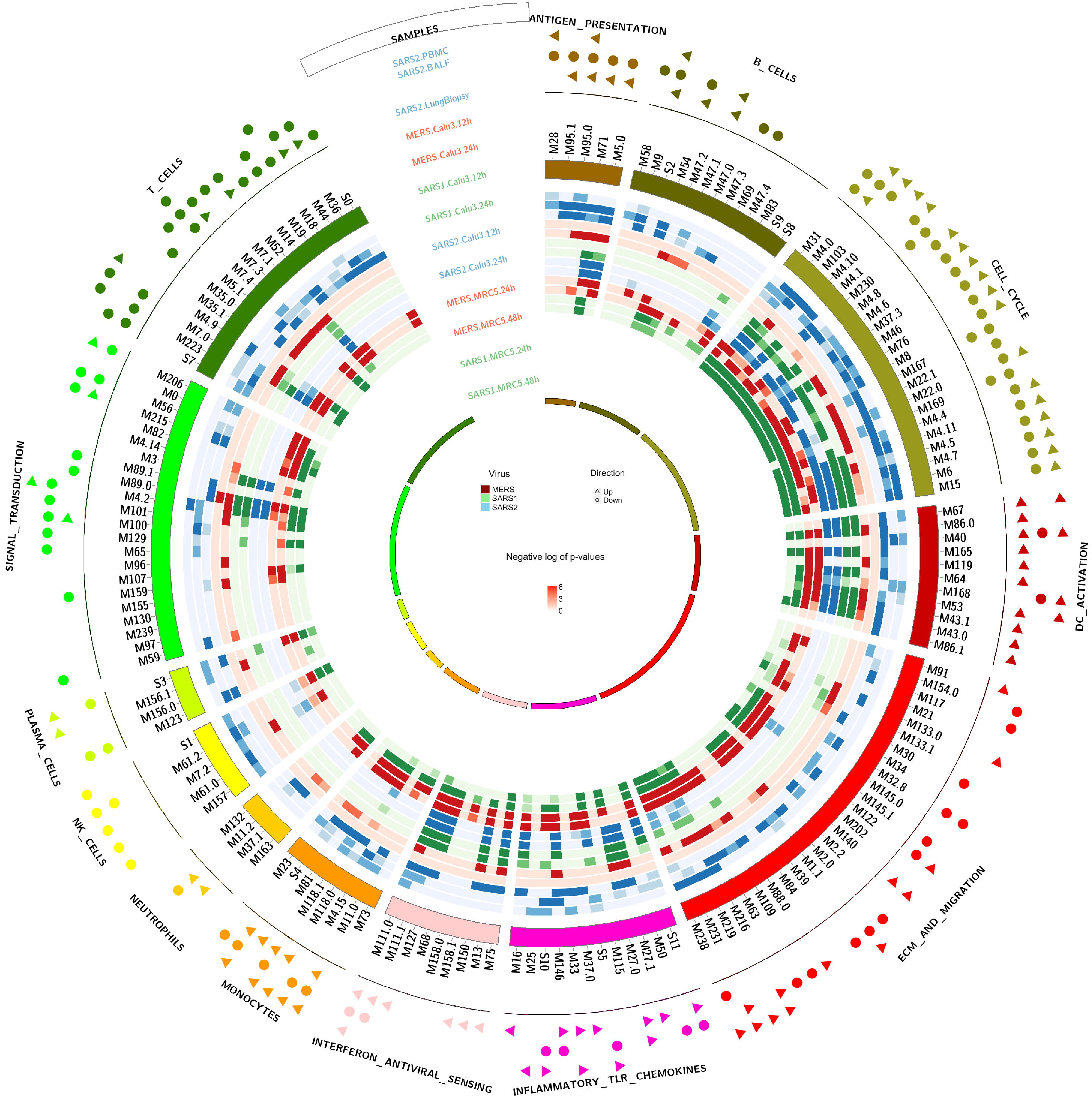
SAMPLES
SARS2.PBMC
SARS2.BALF
SARS2.LungBiopsy
MERS.Calu3.12h
MERS.Calu3.24h
SARS1.Calu3.12h
SARS1.Calu3.24h
SARS2.Calu3.12h
SARS2.Calu3.24h
MERS.MRC5.24h
MERS.MRC5.48h
SARS1.MRC5.24h
SARS1.MRC5.48h
ANTIGEN_PRESENTATION
M28 M95.1 M95.0 M71 M5.0
B_CELLS
M58 M9 S2 M54 M47.2 M47.1 M47.0 M47.3 M69 M47.4 M83 S9 S8
CELL_CYCLE
M31 M4.0 M103 M4.10 M4.1 M230 M4.8 M4.6 M37.3 M46 M76 M8 M167 M22.1 M22.0 M169 M4.4 M4.11 M4.5 M4.7 M6 M15
DC_ACTIVATION
M67 M86.0 M40 M165 M119 M64 M168 M53 M43.1 M43.0 M86.1
ECM_AND_MIGRATION
M91 M154.0 M117 M21 M133.0 M133.1 M30 M34 M32.8 M145.0 M145.1 M122 M202 M140 M2.2 M2.0 M1.1 M39 M84 M88.0 M109 M63 M216 M219 M231 M238
INFLAMMATORY_TLR_CHEMOKINES
M16 M25 S10 M146 M33 M37.0 S5 M115 M27.0 M27.1 M50 S11
INTERFERON_ANTIVIRAL_SENSING
M111.0 M111.1 M127 M68 M158.0 M158.1 M150 M13 M75
MONOCYTES
M23 S4 M81 M118.1 M118.0 M4.15 M11.0 M73
NEUTROPHILS
M132 M11.2 M37.1 M163
NK_CELLS
S1 M61.2 M7.2 M61.0 M157
PLASMA_CELLS
S3 M156.1 M156.0 M123
SIGNAL_TRANSDUCTION
M206 M0 M56 M215 M82 M4.14 M3 M89.1 M89.0 M4.2 M101 M100 M129 M65 M96 M107 M159 M155 M130 M239 M97 M59
T_CELLS
S0 M36 M44 M18 M19 M14 M52 M7.1 M7.3 M7.4 M5.1 M35.0 M35.1 M4.9 M7.0 M223 S7
Virus
MERS
SARS1
SARS2
Direction
△ Up
○ Down
Negative log of p-values
6
3
0